Check for updates

Marine animal forests in high-energy environments after a large anthropic impact: discoveries from the Rion-Antirion Strait, Greece

Lucinda Titri[1]*, Aurélia Hubert-Ferrari[1], Basile Caterina[1], Vasilis Gerovasileiou[2,3], Dimitris Christodoulou[4], Elias Fakiris[5], Xenophon Dimas[4], Maria Geraga[4] and George Papatheodorou[4]

[1]Research Unit SPHERES, Department of Geography, University of Liege, Liège, Belgium, [2]Department of Environment, Faculty of Environment, Ionian University, Zakynthos, Greece, [3]Hellenic Centre for Marine Research (HCMR), Institute of Marine Biology, Biotechnology and Aquaculture (IMBBC), Heraklion, Greece, [4]Laboratory of Marine Geology and Physical Oceanography (Oceanus-Lab), Department of Geology, University of Patras, Patras, Greece, [5]Independent Researcher, Patras, Greece

The Rion−Antirion Strait (Greece, 50−100 m depth) hosts rich Marine Animal Forests (MAFs), formed by several species of anthozoans, sponges, bryozoans and tunicates. Using twelve video transects collected in 2019 and 2023 and a Regional Oceanographic Modelling System (ROMS) hydrodynamic model, we characterized the assemblages' biological composition, geomorphology, and physical drivers. Strong bidirectional bottom currents (0.01−0.25 m/s, peaking at 0.8 m/s) funnel nutrients into the strait, resulting in the highest chlorophyll concentrations recorded between the adjacent Patras and Corinth Gulfs. Bridge construction (1998−2004) likely caused extensive habitat loss through dredging, excavation, ballast dumping, and fine-sediment remobilization. Today, pioneer taxa − such as *Alcyonium* spp. and Caryophylliidae spp. − form dense fields, benefiting from trophic flexibility, rapid recruitment, and tolerance to moderate turbidity. In contrast, fragile and less adaptable taxa such as Antipatharia and Pennatuloidea remain sparse and degraded, suggesting limited recovery potential under sustained disturbance. Sponges and tunicates play a key role in post-disturbance habitat structuring by providing settlement microhabitats. Our results suggest unexpected resilience of anthozoan assemblages in high-energy, non-rocky settings, while underscoring the ecosystem's likely vulnerability to cumulative anthropogenic pressures. The absence of pre-disturbance baseline data limits the reconstruction of historical biodiversity levels, emphasizing the need for long-term monitoring to assess future impacts from coastal infrastructure development and climate change. These findings provide new insights into MAF ecosystem dynamics and inform targeted conservation strategies for vulnerable Mediterranean habitats.

KEYWORDS

anthropogenic impact, sponge-corals-tunicates association, benthic communities, sediment remobilization, biotope resilience, habitat mapping, Eastern Mediterranean Sea

1 Introduction

Marine Animal Forests (MAFs) are complex, three–dimensional benthic ecosystems formed by sessile suspension–feeding invertebrates such as cnidarians (e.g. corals and gorgonians), sponges, bivalve mollusks, and bryozoans (Rossi et al., 2017, 2025 and references therein). These organisms build structural frameworks that create canopy–like habitats, thereby enhancing benthic biodiversity, modulating seabed hydrodynamics, and contributing to essential ecosystem services such as nutrient cycling and carbon sequestration (Rossi et al., 2017; Orejas et al., 2022 and references therein).

In the Mediterranean Sea, many taxa contribute to MAF formation, including species that are legally protected or considered endangered (Rizzo et al., 2025). In Greek waters, MAFs are documented across diverse habitats, reflecting their taxonomic and bathymetric variability (UNEP/MAP–SPA/RAC, 2023; Salomidi et al., 2025; Fabri et al., 2025). Greek MAFs play a key ecological role, providing structurally complex habitats that support biodiversity and ecosystem functions (Rizzo et al., 2025; Johnson and Ferreira, 2025). However, despite being one of the most intensively studied marine basins, the Mediterranean – especially its eastern sector – still harbors under-explored regions, particularly where MAFs occur in low densities, isolation, or under strong anthropogenic pressure (e.g., Taviani et al., 2011; Balogh et al., 2023; Salomidi et al., 2025; Thurstan et al., 2017).

Many MAF–forming taxa, especially cold–water corals, exhibit slow growth rates and very limited capacity for recovery, making them especially vulnerable (Freiwald et al., 2004; Reynaud and Ferrier-Pagès, 2019). Anthropogenic pressures such as bottom trawling, pollution, coastal development, and warming sea temperatures further exacerbate the degradation of MAFs and their associated fauna (Garrabou and Harmelin, 2002; Lartaud et al., 2019; Garrabou et al., 2022; Bramanti et al., 2023; Hinz, 2017). Conservation efforts have intensified in recent years, but protection remains spatially fragmented and often insufficient to ensure the long-term integrity of MAFs across multiple scales (Rizzo et al., 2025; Lauria et al., 2017). Environmental drivers such as hydrodynamics and seabed morphology critically influence MAF spatial distribution and structure, yet their interactions with anthropogenic stressors remain poorly resolved, particularly in transitional or marginal settings (Lo Iacono et al., 2019; Mohn et al., 2023). In this regard, the recently discovered MAF in the Rion–Antirion Strait (Greece) offers a compelling opportunity to explore resilience and responses under combined natural and human pressures. Situated between 50 and 100 m depth in a narrow corridor connecting the Ionian Sea and Gulf of Corinth, the site is characterized by strong bottom currents (>0.5 m/s; Fourniotis and Horsch, 2010), complex geomorphology (Rubi et al., 2022), and substantial anthropogenic alteration due to the presence of a 2 km bridge (Biesiadecki et al., 2004; Apostolopoulos, 2010).

Here, we aim to (i) characterize the structure and composition of the MAF community and associated biotopes, and (ii) evaluate the influence of local 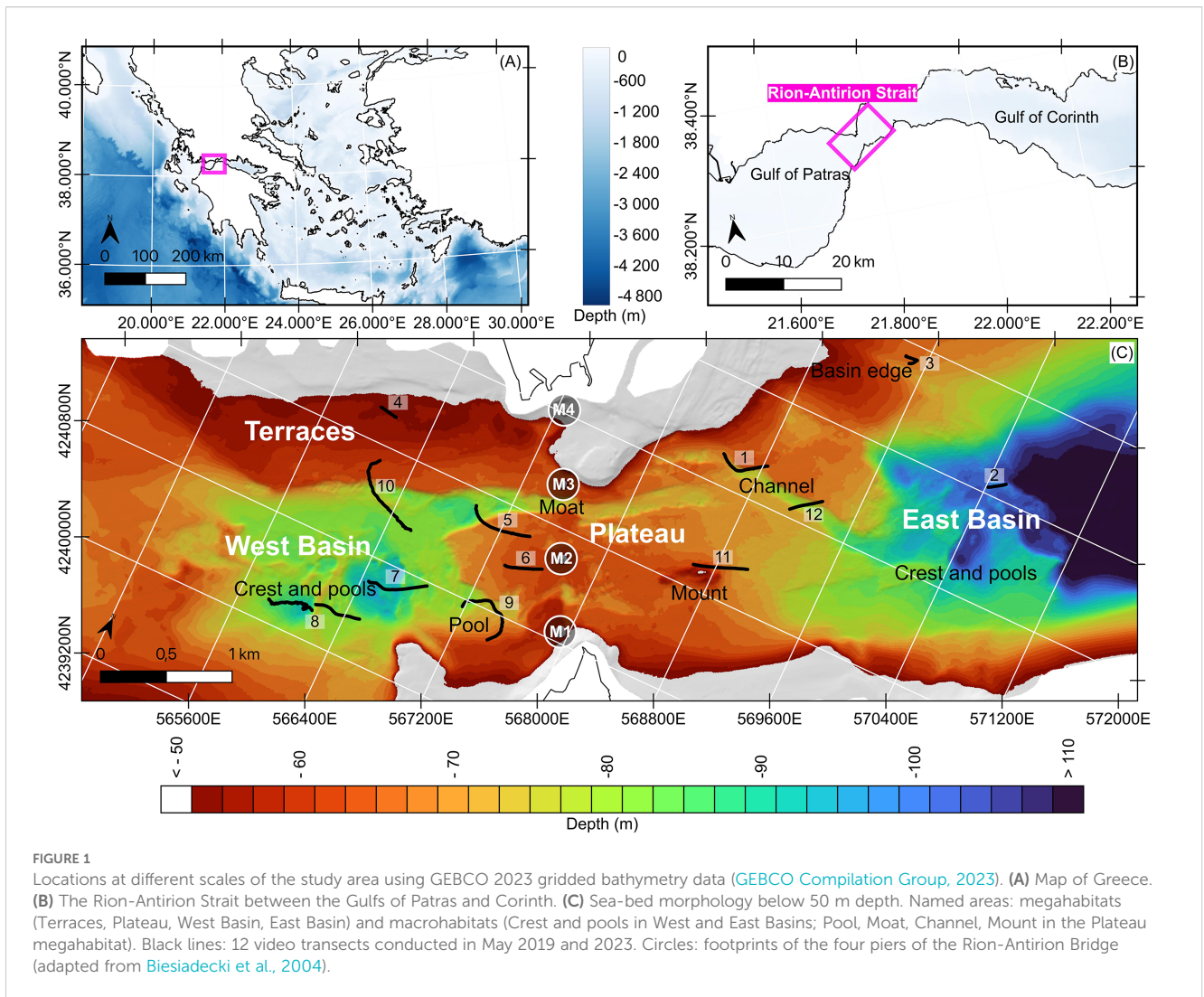hydrodynamic forcing on ecosystem response to human impacts, via field surveys (May 2019, 2023) and hydrodynamic modeling using Regional Oceanographic Modelling System (ROMS).

2 Materials and methods

2.1 Geographical and hydrodynamic setting: the Rion-Antirion Strait

The Rion-Antirion Strait separates the Gulf of Patras (west) and the Gulf of Corinth (east) (Figure 1). The Gulf of Patras is ~80 km long and 20–40 km wide, reaching 140 m depth (Ferentinos et al., 1985). The Gulf of Corinth is ~120 km long, up to 40 km wide, and ~900 m deep. The Strait itself is ~2 km wide and 70 m deep at the bridge location (Rubi et al., 2022). In this narrow, shallow zone, tidal bottom currents are amplified. Bottom currents can reach velocity greater than 1 m/s (Rubi et al., 2022), and are highly dependent on the tidal regime. During flood tide, surface currents flow eastward to the Gulf of Corinth; during ebb tide, they reverse westward to the Gulf of Patras (Caterina et al., 2025). However, bottom water masses behave differently, producing a bidirectional system with internal waves. These waves vary with the semi-diurnal tidal cycle (Rubi et al., 2022; Caterina et al., 2025), and bottom currents may oppose surface flows with velocities up to 3 m/s, compared to ~1 m/s at the surface. Wind, shaped by the surrounding topography and constriction at the Strait, also impacts circulation. Prevailing NW winds (Koletsis et al., 2013) deepen the thermocline (~60 m) and increase mixing, influencing exchange rates across the Strait (Fourniotis et al., 2018; Caterina et al., 2025).

The Strait is a thermal anomaly compared to the adjacent gulfs due to upwelling of cold Corinthian waters (Caterina and Hubert-Ferrari, 2025). Salinity remains stable at ~38.5 ± 0.1 psu throughout (Poulos et al., 1996; Fourniotis and Horsch, 2015; Rubi et al., 2022). There is a seasonal cycle: summer stratification vs. winter mixing (~16°C uniform temperature). In Patras, stratification shows a warm 10 m surface layer (~23°C), a thermocline to 60 m, and stable ~13°C deep water (Friligos et al., 1985). In the Gulf of Corinth, the transition zone can reach >100 m (Anderson and Carmack, 1973; Poulos et al., 1996). Water exchange through the Strait affects local water column parameters. Friligos et al. (1985) documented that the waters were slightly supersaturated in oxygen (O_2 saturation >100%) from 0 to 50 m depth. CTD data from the INTERREG_IONIAN projects (SeaDataNet, 2000) showing temperature, salinity, turbidity, and fluorescence profiles from four stations (two in the strait and two in Patras) provide additional water column parameters. In September, salinity stayed near 38 psu and slightly increased with depth, consistent with literature (Friligos et al., 1985) (Figure 2). The Strait had a thermocline at ~20 m, with surface temperatures at 24°C dropping to 18°C. Patras showed three water layers: 0–20 m (warm), 20–40 m (transition), and below 50 m (stable ~16°C). By March, water columns were mixed (13.5–14°C) (Figure 2). Fluorescence (phytoplankton proxy) peaked below 20 m in

FIGURE 1
Locations at different scales of the study area using GEBCO 2023 gridded bathymetry data (GEBCO Compilation Group, 2023). **(A)** Map of Greece.
(B) The Rion-Antirion Strait between the Gulfs of Patras and Corinth. **(C)** Sea-bed morphology below 50 m depth. Named areas: megahabitats
(Terraces, Plateau, West Basin, East Basin) and macrohabitats (Crest and pools in West and East Basins; Pool, Moat, Channel, Mount in the Plateau
megahabitat). Black lines: 12 video transects conducted in May 2019 and 2023. Circles: footprints of the four piers of the Rion-Antirion Bridge
(adapted from Biesiadecki et al., 2004).

March, and at ~20 m (Strait) and ~50 m (Patras) in September—
consistent with stratification trapping nutrients. Dissolved oxygen
shows maximum values at 20 to 40m water depth. This aligns with
earlier findings (Friligos et al., 1985) on seasonal stratification and
nutrient cycling. Dissolved oxygen trends follow those
of fluorescence.

The Strait's topography reflects both tectonics and hydrodynamic
shaping (Rubi et al., 2022), with rugged bathymetry and a moderately
consolidated substrate shaped by strong erosive currents (Figure 1).
Rubi et al. (2022) describe morphologies linked to bottom currents—
terraces, escarpments, plateaus, channels, moats, and deep pools—
below 50 m depth, in this net erosional environment (Stow et al., 2009).
These are categorized into megahabitats and mesohabitats following Lo
Iacono et al. (2019). Four megahabitats occur below 50 m: a central
plateau (60–70 m depth), two deep basins to the east and west, and
northwestern terraces (Figure 1). These larger structures host a range of
mesohabitats. On the plateau east of the bridge, two mesohabitats are
distinguished: (1) a mound (420 m long, 150 m wide, 15 m high) and
(2) a fluvial channel (1.6 km long, 100–270 m wide, 4-6m deep) (Rubi
et al., 2022; Figure 1). To the west of the bridge, two more mesohabitats
are found on the plateau: (3) a northern straight moat formed by

bottom currents (2 km long, 140–240 m wide, 3–21 m deep); (4) a
southern elongated pool (1 km long, 300 m wide, 95–100 m deep).
Additional mesohabitats in the West and East Basins are defined by
their rugged morphologies, including deep pools and crests (Rubi
et al., 2022).

Sediments vary across the Strait, reflecting lithology, induration,
and tectonic deformation. The basement rocks are not exposed at
the seafloor at depths below 500 m (Biesiadecki et al., 2004). The
most resistant unit is the indurated, coarse-grained, flat sedimentary
layer capping the plateau. Boreholes near the bridge show a gradual
northward thinning of the indurated cap, underlain by clay-rich
sediments (Biesiadecki et al., 2004; Rubi et al., 2022). Consequently,
the two megahabitats incised in the plateau west of bridge differ
slightly in lithology: the northern moat is partly carved in clay-rich
sediments, whereas the southern pool remains confined to the
coarse-grained cap. Terraces are composed of a different, laterally
variable sedimentary unit, younger and probably less indurated,
with finer materials toward the north (Piper and Panagos, 1979;
Rubi et al., 2022). The western basin is an erosional structure
formed in older, indurated, and deformed sediments. Seismic
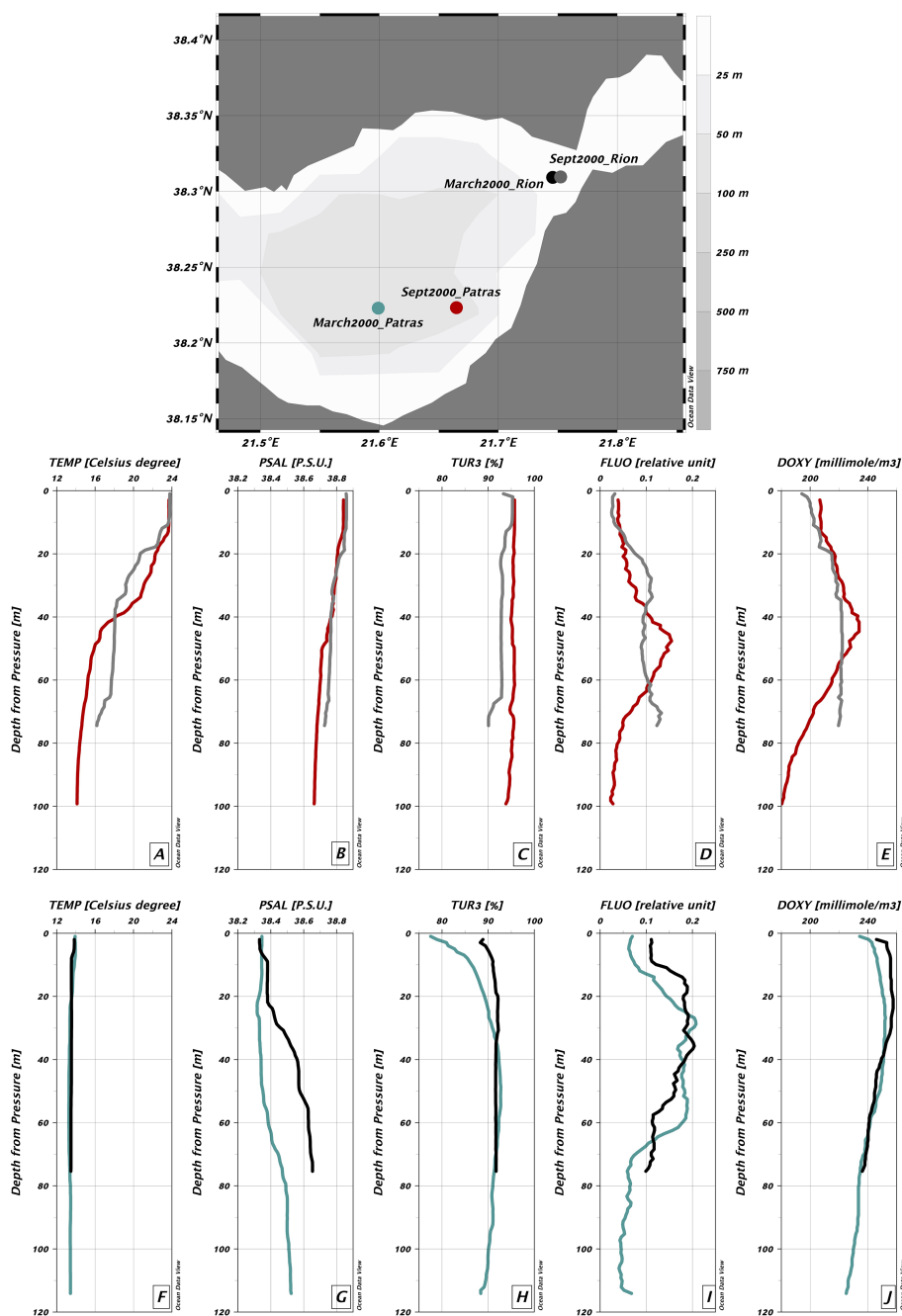reflection data suggest fine-grained facies deposited in

FIGURE 2
Water column parameters measured using CTD profiles: temperature (°C), practical salinity (psu), turbidity (%), fluorescence (relative units), and dissolved oxygen (mmol/m³). The map shows the measurement locations. Colored dots correspond to selected CTD stations. **(A–E)** September 2000: 26 Sept. 2000, 12:30, Patras (red); 26 Sept. 2000, 14:25, Rion (grey). **(F–J)** March 2000: 26 March 2000, 12:30, Patras (green); 26 March 2000, 17:05, Rion (black).

pre-Holocene lacustrine to marine conditions. The eastern basin is similar but composed of non-deformed pre-Holocene sediments, with Holocene deposits lining its edges (Beckers et al., 2016; Rubi et al., 2022). These finer-grained materials in the basins are more erodible than the coarser-grained cap of the plateau, which is why erosion was more limited there.

The Strait's seabed shows major anthropogenic impacts despite its no-fishing status. Two main sources are submarine cables and

the Rion-Antirion Bridge. According to the Navionics® maps (Navionics®, 2024), at least seven cables cross the plateau, and the true number may be higher. At least one WWII metallic shipwreck is resting on the plateau providing substrate for ecosystems. A potentially much greater disruption stems from the construction of the 2,252 m-long Rion-Antirion Bridge. Its design posed exceptional engineering challenges (Combault et al., 2000) due to deep water, weak substratum, strong seismicity, and fault

activity (Beckers et al., 2015). Environmental impact began before construction with subsurface surveys in 1988–1992 and intensified in 1996 (Biesiadecki et al., 2004). The eastern shore of the Antirion peninsula was heavily modified to accommodate a temporary seaport and dockyard for bridge component assembly. Pylon site preparation began in 1998; pylon construction occurred in 2000. The bridge includes two approaches (392 m and 239 m) and four piers separated by 560 m. The bridge was inaugurated on 7 August 2004 (Biesiadecki et al., 2004; Apostolopoulos, 2010). Major disturbances occurred at the four 90 m-wide pier locations. Prior to construction, subsurface drilling and testing disrupted the seafloor at each pier site, and electric cables were relocated (Biesiadecki et al., 2004). During construction, the seafloor was levelled at each pier using remotely operated dredging vehicles. Below and around piers M1–M3, the soil was reinforced with 20 mm thick, 2 m diameter steel pipe inclusions (25–30 m long, spaced ≥7 m apart) to prevent liquefaction (Combault et al., 2000). These 3 piers rest directly on a 3-m-thick filter and gravel ballast layer (Biesiadecki et al., 2004). The ballast and steel inclusions were installed from a purpose-built barge, stabilized by four 700-ton counterweights and a tension leg system—potential sources of disturbance. At Pier M4, soils were excavated to reach deeper gravels, eliminating the need for inclusions. These operations likely resulted in considerable environmental disruption.

2.2 Data acquisition and identification

There were two data acquisition campaigns: May 2019 and May 2023. For this study, we used 2019 MBES (multibeam echosounder) data proceeded and interpreted by Rubi et al. (2022), together with video footage from both 2019 and 2023. MBES data was used to generate a 5 m × 5 m bathymetric grid covering 211 km², which Rubi et al. (2022) used to identify megahabitats and mesohabitats (km to 10 m), while macro- and microhabitats (10 m to <1 m) were identified here from video footage. Video footage was the only way to characterize the biotope, as the study area shows strong and variable bottom currents (Rubi et al., 2022; Caterina et al., 2025), that prevent the use of ROVs (Remotely Operated Vehicle) or *in situ* sampling. Consequently, seabed images were acquired using a Towed Underwater Camera System (TUCS). Twelve (12) video transects were carried out along the various seabed types and particularly within the megahabitats and mesohabitats of the survey area. In 2019, the camera had a resolution of 640x480, while in 2023, an HD camera (1920x1080) was used. During both campaigns, the boat drifted at a constant speed of 1–2 knots. In 2019, biotope image acquisition consisted of seven transects (Figure 1; see Table 1). GPS coordinates (accurate to ~10 cm) were embedded in the videos and correspond to the boat's position. Recordings were made on 20 May at 9:21 am, 10:29 am, 11:03 am, 1:45 pm, 1:56 pm, 2:18 pm, and 2:42 pm. The 2023 acquisition was conducted from 12 to 26 May with five transects recorded on 24 May at 11:25 am, 12:15 pm, 12:31 pm, 1:41 pm, 2:13 pm, 3:09 pm, and 3:32 pm, with the first three grouped as a single profile (Figure 1; Table 1). GPS coordinates, recorded every second, correspond to the boat's position. Coral positions along transects may deviate by over one meter due to the flexible, non-rigid cable linking the boat and the camera. Transects are named after the acquisition start time (Table 1).

The marine biotopes and associated assemblages in the Rion-Antirion Strait (i.e., corals, sponges and tunicates) were identified by video analysis. Each video was viewed more than four times, frame-by-frame. MAF locations were mapped using QGIS software.

TABLE 1 Characteristics of profiles realized. Coordinates are given in UTM zone 34N.

Numbering in Figure 1	Name of corresponding profile	Profile length (in m)	Start Y (Northing, UTM 34N)	Start X (Easting, UTM 34N)	Start depth (m)	End Y (Northing, UTM 34N)	End X (Easting, UTM 34N)	End depth (m)	Profile direction
1	2019-05-20_9.21	400	4242633.14	568492.17	70	4242689.2	568834.8	68	eastward
2	2019-05-20_10.29	120	4243251.09	570417.24	100	424328.5	570531.7	100	eastward
3	2019-05-20_11.03	150	4243849	569476.4	70	4243891.5	569431.5	68	/
4	2019-05-20_13.45	150	4241851.1	565982.4	56	4241830.9	566119	54	/
5	2019-05-20_13.56	500	4241481.5	566953.5	80	4241440.6	567422.9	60	eastward
6	2019-05-20_14.18	275	4241161.7	567342.8	66	4241256.8	567613.4	62	eastward
7	2019-05-20_14.42	450	4240612.6	566456.7	100	4240770	566872.9	80	eastward
8	2023-05-24_11.25_12.15 and 2023-05-24_12.31	460 and 360	4240169.9	565826.5	80	4240324.7	566513.7	80	eastward
9	2023-05-24_13.41	700	4240592.4	567459.9	60	4240741.4	567181.1	82	northward
10	2023-05-24_14.13	630	4241102.2	566580.9	80	4241483.9	566145.8	60	northward
11	2023-05-24_15.09	415	4241772.5	568636.7	60	4241913.4	569026.6	74	eastward
12	2023-05-24_15.32	380	4242464.1	569122.4	74	4242621.4	569324	70	eastward

As no physical samples were collected, identification was based exclusively on visual characteristics following a non-invasive approach. We relied on databases and current literature sources documenting benthic invertebrates from similar environments in various ecoregions of the Mediterranean Sea (e.g., Álvarez-Pérez et al., 2005; Salomidi et al., 2006; Kefalas and Castritsi-Catharios, 2007; Taviani et al., 2017; Rueda et al., 2019; Otero and Mytilineou, 2022; André et al., 2023; Balogh et al., 2023; Fournier et al., 2023; Stamouli et al., 2023). Nevertheless, this method limits accurate species-level identification, which typically requires microscopic

analysis of physical samples. Summaries of identified benthic species are found in Tables 2, 3.

2.3 Chlorophyll concentration mapping and hydrodynamics modeling

Chlorophyll concentration (CHL) was mapped using Copernicus satellite data (Copernicus Marine Service, 2025a), exported as NetCDF files and processed with Julia (Barth, 2024;

TABLE 2 Summary of observed taxa (excluding anthozoans).

Taxon (Potential ID)	Morphology and size	Depth (Strait)	Substrate type	Local distribution (Profiles)	Observed associations	Key references #
Sponges						
Axinella spp. and/or *Ulosa digitata*	Red-orange, branched, 10–20 cm	~60m	Rocky walls	Profiles 1 (104), 12 (7); lower W (e.g., 5/6: 12, 10: 15)	Other sponges, bryozoans	Stamouli et al., 2023
Axinyssa spp.	Yellow-orange, irregular, 10–15 cm diameter, 1–2 cm height	60-80m	Hard substrate	Profile 8	Other orange sponges	Salomidi et al., 2006; Kefalas and Castritsi-Catharios, 2007; Stamouli et al., 2023
Agelas oroides	Bright orange, lobed, up to 20 cm diameter, 1 cm height	60-80m	Hard substrate	Profile 8	Yellow and blue encrusting sponges	Salomidi et al., 2006; Kefalas and Castritsi-Catharios, 2007; Stamouli et al., 2023;
Tethya citrina	Spherical, 5–10 cm diameter, granular, yellow	60-80m	Hard substrate	Profile 8	Not observed	Stamouli et al., 2023; Digenis et al., 2024
Dictyoceratida spp.	Brown/black, globular, ~10 cm, irregular surface	60-80m	Hard substrate	Profile 10	Not observed	Stamouli et al., 2023
Tunicates						
Phallusia sp.	Black tubular, ~10 cm	70m	Hard substrate	Profiles 1, 10 (north)	Not observed	André et al., 2023
Halocynthia papillosa	Red, bag-like, white spots, 6–8 lobes, up to 20 cm	50-80m	Shaded hard substrate	Observed in many profiles incl. 8	Possibly sponges	Salomidi et al., 2006; André et al., 2023
Ascidia mentula	Oval, 5–10 cm, white-spotted siphons	60-80m	Hard substrate	Profile 8	Sponges (Figure 5A-D)	Rowley, 2008
Bryozoans						
Adeonella or *Smittina* or *Myriapora truncata*	Orange-red, bushy, cylindrical branches, few cm	50-80m	Hard substrate	Profiles 1, 7, 8, 12; dead in West Basin	*Axinella* spp., *Agelas oroides*	Berning, 2007; Rueda et al., 2019
Holothuroidea						
Parastichopus regalis	–	60-80m	Hard substrate	2 observed, profile 8	Not observed	–
Teleostei						
Serranus cabrilla	–	60-80m		Scattered individuals, profile 8	Not observed	–
Asterozoa						
Peltaster placenta	–	~60m	Hard substrate	Several observed, profile 11	Not observed	–
Echinaster sepositus	–	~60m	Hard substrate	Several observed, profile 11	Not observed	–
Ophiuridae spp.	–	~60m	Hard substrate	Several observed, profile 11	Not observed	–

TABLE 3 Summary of observed anthozoans.

Taxon (Potential ID)	Morphology and size	Depth (Strait)	Substrate type	Local distribution (Profiles)	Observed associations	Key references
Alcyonium spp. (likely *A. palmatum*)	Stubby, finger-like branches; polyps evenly distributed. White and red morphs. Size: few cm (*in situ*); 10–50 cm (lit.)	~60m	Hard and soft	Mostly west of the bridge: dense fields in the western plateau, pool macrohabitat, and West Basin (5, 6, 7, 9). One record east (2).	Small sponges	Ambroso et al., 2013; Grinyó et al., 2020; Balogh et al., 2023; Fournier et al., 2023
Caryophylliidae spp.	Cylindrical encrusting cups, small polyps. Patchy colonies atop anthozoan/bryozoan debris.	60-100m	Hard (debris mounds)	99 occurrences: 1 (9), 6 (1), 8 (37), 9 (4), 10 (22), 11 (22), 12 (4)	Sponges, occasionally tunicates	Álvarez-Pérez et al., 2005; Salomidi et al., 2006; Taviani et al., 2017; Rueda et al., 2019; Otero and Mytilineou, 2022; Balogh et al., 2023; Fournier et al., 2023
Antipatharia spp. (likely *Antipathella subpinnata*)	Bushy/fan-shaped colony. Thin, irregular white branches, no distinct pinnules. Often broken; <10 cm	80-60m	Hard	1 (5), 9 (5), 11 (9)	–	Mytilineou et al., 2014; Rueda et al., 2019; Otero and Mytilineou, 2022; Balogh et al., 2023; Fournier et al., 2023
Pennatuloidea spp. (likely *Cavernularia* cf. *pusilla* and *Pteroeides griseum*)	Central stalk with polyps. *C. pusilla*: compact (~4 cm), closely spaced polyps. *P. griseum*: elongated (up to 20 cm), feather-like arrangement.	60-90m	Soft	*C.* cf. *pusilla*: 1 (7); *P. griseum*: 1 (4), 2 (3), 3 (1), 8 (5). Present in 1, 2, 3, 4, 8, 10.	–	Salomidi et al., 2006; Taviani et al., 2017; Rueda et al., 2019; Otero and Mytilineou, 2022; Balogh et al., 2023; Fournier et al., 2023
Parazoanthus axinellae	Yellow, low encrusting colonies on cobbles or sponges. Cylindrical tentacled polyps with connecting tissue.	~80m	Hard	1 (7), 7 (1), 8 (1), 1 (9)	Often encrusting sponges or cobbles	Garrabou, 1999; Salomidi et al., 2009; Rueda et al., 2019; Balogh et al., 2023

Caterina and Hubert-Ferrari, 2025). An initial quality check was performed by filtering out days with more than 95% missing pixels, which were considered unusable. The remaining dataset, spanning 2008 to 2022, was studied over the Patras and Corinth Gulfs. The analysis involved creating daily maps to obtain the spatial distribution of CHL, followed by the generation of a spatially averaged map over the entire domain and period. In this way, each pixel represents the time average across the whole period, without applying any interpolation (Caterina & Hubert-Ferrari, 2025).

Bottom current modeling was performed using ROMS (Regional Ocean Modeling System; Shchepetkin and McWilliams, 2009; Moore et al., 2011). ROMS is a highly configurable, free-surface, terrain-following hydrodynamic model designed for simulating oceanic processes (Shchepetkin and McWilliams, 2005), and was applied here to improve understanding of currents in the Rion-Antirion Strait as in Caterina et al. (2025).

The model domain covered the strait area from Patras to the Corinth Gulf (21.65°–22°E, 38.2°–38.45°N), with open boundaries east and west and closed boundaries north and south. The ROMS bathymetric grid was built at the GEBCO resolution of 450 m (GEBCO Compilation Group, 2024). This grid was manually corrected in the Strait area by digital adjustment of pixels to better fit the bathymetry described in Rubi et al. (2022). The specific ROMS grid parameters were as follows: Tcline = 50 m (width of surface or bottom boundary layer requiring higher vertical resolution during stretching), θs = 5 (S-coordinate surface control

parameter, 0<= θs <= 10), θb = 4 (S-coordinate bottom control parameter, 0 <= θb <= 4), nlevels = 32 (number of vertical adaptative layers). The vertical transformation equation used was the improved formulation of Shchepetkin (2005) (Eq. 2 in WikiROMS, 2019, derived from Shchepetkin and McWilliams, 2005), while vertical stretching followed the improved double stretching function of Shchepetkin (2009) (Eq. 2.3 for the surface and Eq. 2.4 for the bottom; Shchepetkin and McWilliams, 2009), as applied in Caterina et al. (2025).

The preparation of the initial grid for ROMS input was carried out using Julia scripts (Barth, 2025), where all the inputs are retrieved from the Copernicus Marine Service (CMEMS), the General Bathymetric Chart of the Oceans (GEBCO), the European Centre for Medium-Range Weather Forecasts (ECMWF) and the Oregon State University (OSU) Tide Model (TPXO). From the CMEMS, data for the temperature, the salinity, the sea surface elevation and currents movements were retrieved (Copernicus Marine Service, 2025b). The winds were extracted from the ECMWF database for the given period (Barth, 2024; ECMWF, 2018). The tidal initial parameters were extracted from the TPXO Tidal Model (Egbert and Erofeeva, 2002) to fit the boundaries of the ROMS grid (methodology from Caterina et al., 2025).

The model covered May 2019, for which observational data were available to validate the simulations (Rubi et al., 2022). Model outputs were analyzed using Julia (Barth, 2025). The main outputs were velocity maps showing mean scalar velocity (color) and vector velocity (arrows), along with analogous maps for maximum velocity.

In addition, time series of eastward ("u") and northward ("v") velocities were extracted at a grid point (38.32°N, 21.78°E) representing the strait center, in order to analyze current orientations.

3 Results

3.1 Occurrence and distribution of anthozoans

The following anthozoan species were identified, falling into two classes: (1) Hexacorallia: Caryophylliidae spp., *Parazoanthus axinellae* (Schmidt, 1862) and Antipatharia spp. – potentially *Antipathella subpinnata* (Ellis & Solander, 1786); and (2) Octocorallia: *Alcyonium* spp. (likely *Alcyonium palmatum* Pallas, 1766), and sea pens of the superfamily Pennatuloidea including *Pteroeides griseum* (Bohadsch, 1761) and Veretillidae spp. – potentially *Cavernularia* cf. *pusilla* (Philippi, 1835), following standard taxonomic classification schemes (WoRMS Editorial Board, 2025). Figure 3 summarizes the distribution of anthozoans across profiles. *Alcyonium* dominated west of the bridge, while Pennatuloidea spp. were more frequent eastward. Caryophylliidae spp. and Anipatharia spp. were more scattered and occurred at lower densities. Below, we provide morphological descriptions and local distributions of each taxon.

The most widespread anthozoan belonged to genus *Alcyonium* (Octocorallia, Malacalcyonacea, Alcyoniidae), identified by its stubby, finger-like branches a few centimeters tall, with polyps evenly distributed across the surface (Figures 4G–I, 3). Both white and, more rarely, red individuals were observed. This morphology matches *A. palmatum*, reported at depths ranging from 10 to 200 m, on both soft and hard substrates, with a size ranging from 10 to 50 cm (Ambroso et al., 2013; Grinyó et al., 2020; Fournier et al., 2023). In the Strait, *A. palmatum* was especially abundant west of the bridge, where it formed dense fields (<10 cm spacing) (Figure 4G), particularly in the western plateau and its pool macrohabitat, as well as in parts of the west basin (profiles 5, 6, 7, 9; Figure 3). East of the bridge, only a single occurrence was recorded (profile 2; Figure 3). These anthozoans were typically accompanied by diverse smaller sponges.

Scleractinians of the family Caryophylliidae (Hexacorallia, Scleractinia), the second most abundant taxon, were identified by their cm-sized cylindrical encrusting cups with small polyps (Figures 4A, B). They generally appeared as small, patchy colonies on top of mounds of accumulated coral and bryozoan debris. In the Strait, 99 occurrences were recorded (9 in profile 1, 1 in profile 6, 37 in profile 8, 4 in profile 9, 22 in profile 10, 22 in profile 11, and 4 in profile 12; Figure 3). They tended to co-occur with sponges and occasionally tunicates. Their true frequency may be underestimated due to small size, water turbidity, and resolution limits.

A bushy or fan-shaped coral colony, likely belonging to Antipatharia (Hexacorallia) (Figures 4C, D), was also present – potentially *Antipathella subpinnata* – although the video resolution did not allow confident identification. It had numerous thin, irregular white branches la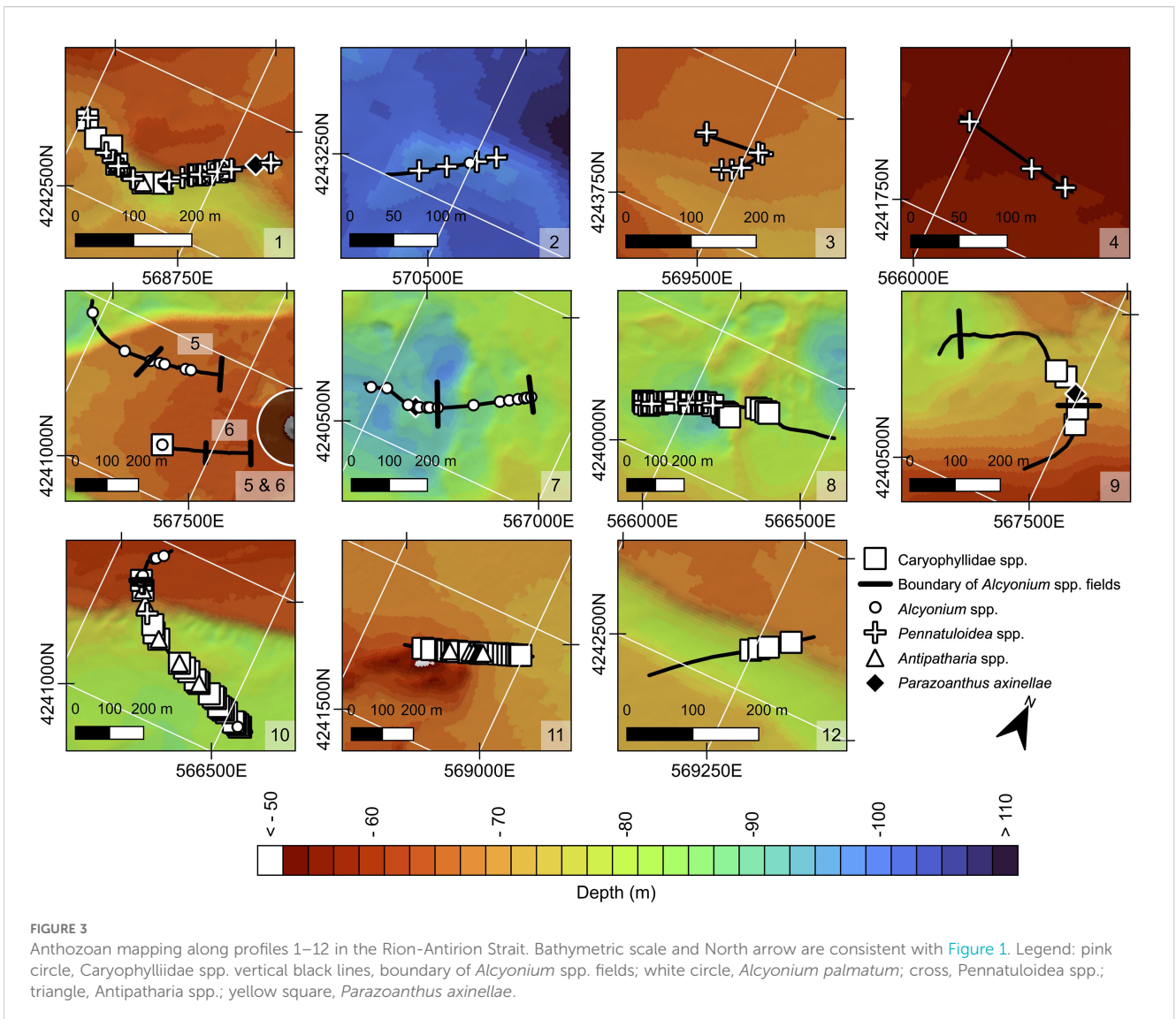cking distinct pinnules. In the Strait, they were generally under 10 cm, often broken, and sparsely distributed (5 in profile 9, 5 in profile 1, and 9 in profile 11; Figure 3).

Sea pens belonging to superfamily Pennatuloidea (Octocorallia, Scleralcyonacea), were also identified (Figure 4E). They are characterized by an elongated central stalk with polyps arrayed along it, anchored by a small peduncle. The smaller morphotype, identified as *Cavernularia* cf. *pusilla*, with closely spaced rows of polyps and a compact form (~4 cm high), was observed in profile 1 (7 individuals) (Figure 3). A larger and more elongated morphotype (up to 20 cm), inferred to be *Pteroeides griseum* was recorded in profiles 1 (4), 2 (3), 3 (1), and 8 (5) (Figure 3). In the Strait, sea pens were more broadly distributed than other taxa across sediment-covered habitats, notably in the east basin (profiles 2 and 3), northern terrace (profile 4), and western macrohabitats (profiles 1, 8, 10), forming the only anthozoan group on fine-grained sediments (Figure 3).

Lastly, a yellow zoantharian forming dense, low colonies encrusting cobbles or sponges was identified as *Parazoanthus axinellae* (Hexacorallia, Zoantharia, Parazoanthidae) (Figure 4F). Polyps formed dense colonies of cylindrical, tentacled individuals connected by shared tissue (Garrabou, 1999). A total of 9 P. *axinellae* occurrences were recorded in the study area (7 in profile 1, 1 in profile 7, and 1 in profile 9; Figure 3).

3.2 Occurrence and distribution of other sessile taxa

Other invertebrate taxa are described below by major taxonomic group, with notes on morphology, abundance, and co-occurrence with other taxa across the study area. Sponges were the most frequent organisms forming marine animal forests on the seafloor (Figures 5A, D), with highly variable densities. Sponge occurrence was very low along the eastern basin edges (profile 3) and northern terraces (profile 4). In contrast, plateau megahabitats-particularly the mount macrohabitat (profile 11), the channel's northwest (profile 1), and the eastern part of the western basin (profile 7) showed high sponge abundance. The largest individuals, likely *Axinella* spp. and/or *Ulosa digitata* (Schmidt, 1866), were red-orange in color and had an arborescent-branched shape (Figure 5A). They were more abundant in the east channel macrohabitat (profile 1), occurring roughly every 10 m on its rocky walls (104 individuals in profile 1; 7 in profile 12), with sizes ranging from 10 to 20 cm in height. West of the bridge, individuals were usually smaller and less branched (e.g., 12 in profiles 5 and 6, 15 in profile 10). *Axinella* spp. often co-occurred with other sponges and bryozoans in the study area (Figure 5G). Yellow-orange sponges with pillow-like, irregular shapes (~10–15 cm diameter, few cm height) were also recorded, with some of them possibly belonging to the genus *Axinyssa* or other members of the family Halichondriidae (order Suberitida) (Figure 5B). In the Strait, they often coexisted with other orange sponges (Figure 5C). Bright, massive orange sponges with lobes up to 20 cm in diameter possibly belonged to the species *Agelas oroides* (Schmidt, 1864) (Figure 5C). In the Strait, A. *oroides* co-occurred with unidentified yellow and blue encrusting sponges (Figures 5B, O). Another sponge, spherical in

FIGURE 3

Anthozoan mapping along profiles 1–12 in the Rion-Antirion Strait. Bathymetric scale and North arrow are consistent with Figure 1. Legend: pink circle, Caryophylliidae spp. vertical black lines, boundary of *Alcyonium* spp. fields; white circle, *Alcyonium palmatum*; cross, Pennatuloidea spp.; triangle, Antipatharia spp.; yellow square, *Parazoanthus axinellae*.

shape, with 5–10 cm diameter, a broad oscule and a granular "citrus peel" surface, was observed, most likely belonging to the species *Tethya citrina* Sarà & Melone, 1965 (Figure 5D). In the Strait, *Tethya* showed no strong associations with other species. Globular brown to black sponges, with irregular surfaces, probably belonging to the order Dictyoceratida (Figure 5I), were also observed.

Bryozoans were also frequently observed in several profiles, with colony morphology and size varying across sites. One of the most common species (possibly belonging to the genera *Adeonella* or *Smittina* or eventually *Myriapora)* was characterized by its bushy, branching orange-red form, with cylindrical branches a few mm in diameter and irregular surfaces. Small colonies, few cm high, were seen in profiles 1 and 12, while larger and more complex bushy forms occurred in profiles 1, 7, and 8. Numerous dead branches, belonging to the same genera, were also recorded in the west basin (Figure 5G).

Tunicates were also identified on indurated substrates at various depths. They were especially common in the channel macrohabitat (profile 1; northern profile 10), the pool macrohabitat (profile 9),

and in the west basin (profile 8). In profile 8, higher densities were observed on the crests. Three tunicate taxa were visible: *Halocynthia papillosa* (Linnaeus, 1767) (Figure 5E); a tubular, black tunicate (~10 cm) (Figure 5H); and the third species, likely *Ascidia mentula* Müller, 1776, had an oval shape with white-spotted siphons – sometimes displaying color variation with depth (Rowley, 2008) – measured 5–10 cm (Figure 5F), and co-occurred with sponges (Figures 5A–D).

3.3 Occurrence of motile taxa

Some motile taxa, including echinoderms and fishes, were also observed although in lower abundances. These included the holothurian *Parastichopus regalis* (Cuvier, 1817) and the asterozoans *Echinaster* (*Echinaster*) *sepositus* (Retzius, 1783), *Peltaster placenta* (Müller & Troschel, 1842), and *Ophiuridae* spp. in profile 11 (Figures 5J–M); as well as a few Teleostei, such as *Serranus cabrilla* (Linnaeus, 1758) in profile 8.
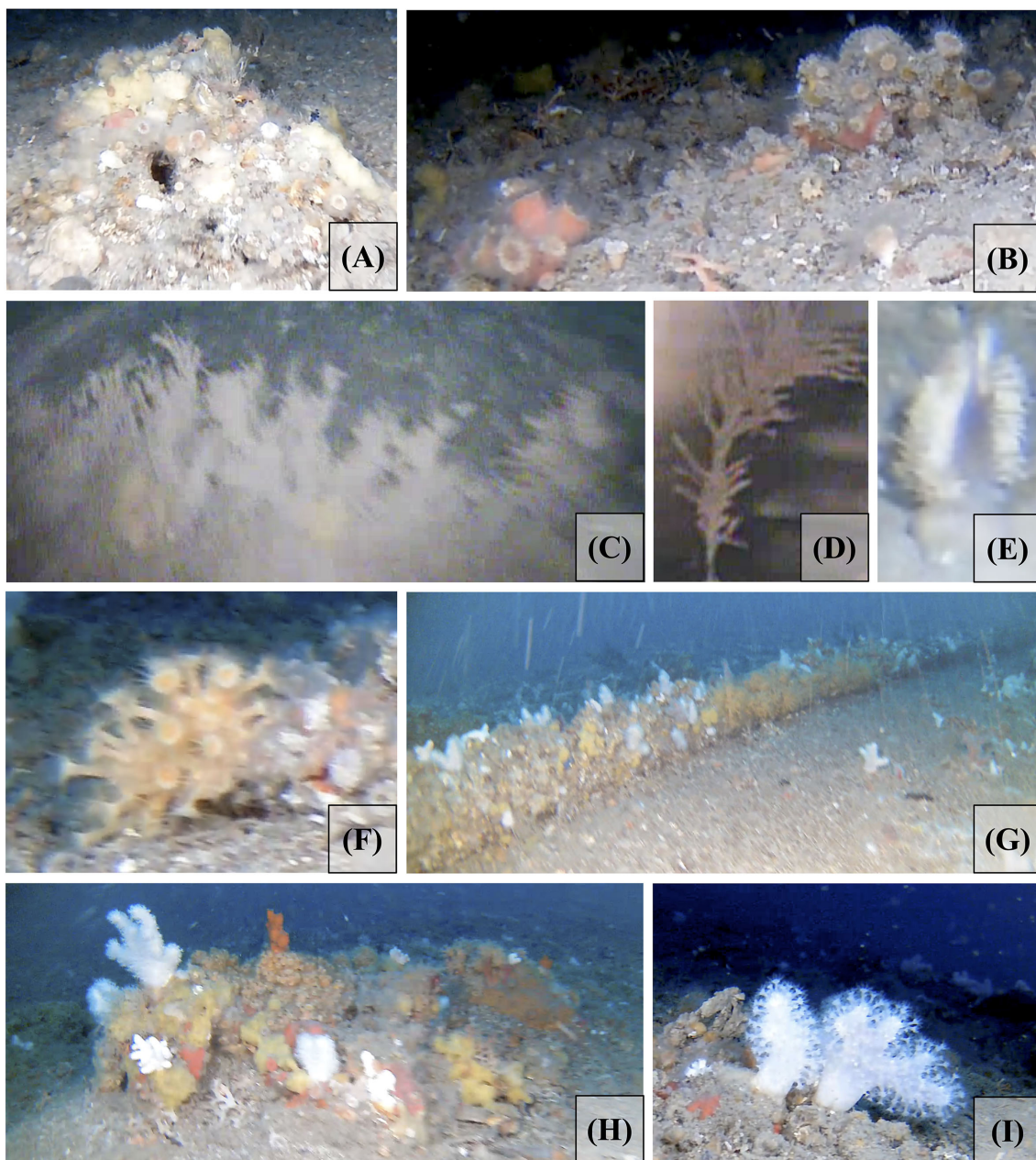
FIGURE 4
Photographs of anthozoan species found in the Rion-Antirion Strait area. **(A)** Caryophylliidae spp. (1) (profile 10). **(B)** Caryophylliidae spp. (2) (profile 8).
(C) Antipatharia framework (possibly *Antipathella subpinnata*) (1) (profile 5). **(D)** Dead Antipatharia (2) (profile 1). **(E)** Pennatuloidea spp. – possibly
Pteroeides griseum (profile 8). **(F)** *Parazoanthus axinellae* (profile 9). **(G)** *Alcyonium* spp. associated with sponges on a submarine cable (profile 9). **(H)**
Assemblage of anthozoans and sponges including *Alcyonium* spp. on the top of a mound (profile 9). **(I)** *Alcyonium palmatum* in a field area (profile 9).

3.4 Sea-bed morphology, substrate type and corals-sponges-bryozoan biotope

Video transects enabled a detailed characterization of seabed morphology, biotopes and associated assemblages within the four megahabitats and their nested macrohabitats in the Rion-Antirion Strait. Variations in substrate type, depth, and topographic complexity strongly influence the spatial distribution and density of benthic communities (Figures 1, 6).

In the west basin, characterized by crest and pool macrohabitats (profiles 8 and 7) at 80–100 m, the seabed consisted primarily of biogenic rubble – dead coral branches, mollusk shells, bryozoan debris, and lithic fragments – predominantly carbonate in composition (Piper and Panagos, 1979) (Figure 3). Grain sizes range mainly from pebbles to cobbles, with rare boulders (Piper and Panagos, 1979). Present-day coral and sponge colonization is heterogeneous and overall sparse (Figure 3), contrasting sharply with the continuous rubble substrate. The eastern part of profile 8 is

FIGURE 5
Photographs of the most common non-anthozoan species observed in the Rion-Antirion Strait area, with corresponding Towed Underwater Camera System (TUCS) profile numbers. **(A)** *Axinella* sp. (profile 1). **(B)** yellow sponges – possibly *Axinyssa* spp. (profile 8). **(C)** *Agelas oroides* (profile 8). **(D)** *Tethya citrina*. (profile 8). **(E)** *Halocynthia papillosa* (profile 10). **(F)** *Ascidia* sp. (profile 8). **(G)** Erect Bryozoa (profile 5). **(H)** *Phallusia* sp. (profile 11). **(I)** Black sponges – possibly Dictyoceratida (profile 10). **(J)** *Serranus cabrilla* (profile 10). **(K)** *Peltaster placenta* (profile 11). **(L)** *Echinaster sepositus* (red) and Ophiuridae sp. (brown and white) (profile 11). **(M)** *Parastichopus regalis* (profile 8).

barren, overlain by a thin veneer of fine sediment and containing only well-preserved biogenic debris. Its western end hosted scattered sponge species (e.g., *Axinyssa* spp., *Agelas oroides*, *Tethya citrina*, and blue encrusting sponges), solitary ascidians (e.g., *Ascidia mentula*), and anthozoans such as Caryophylliidae spp., Pennatuloidea spp. and *Parazoanthus axinellae* (Figures 5B, C, 4B–F, 6). Profile 7 showed greater habitat complexity with small mounds and boulders; a 250 m-long field dominated by *Alcyonium palmatum*
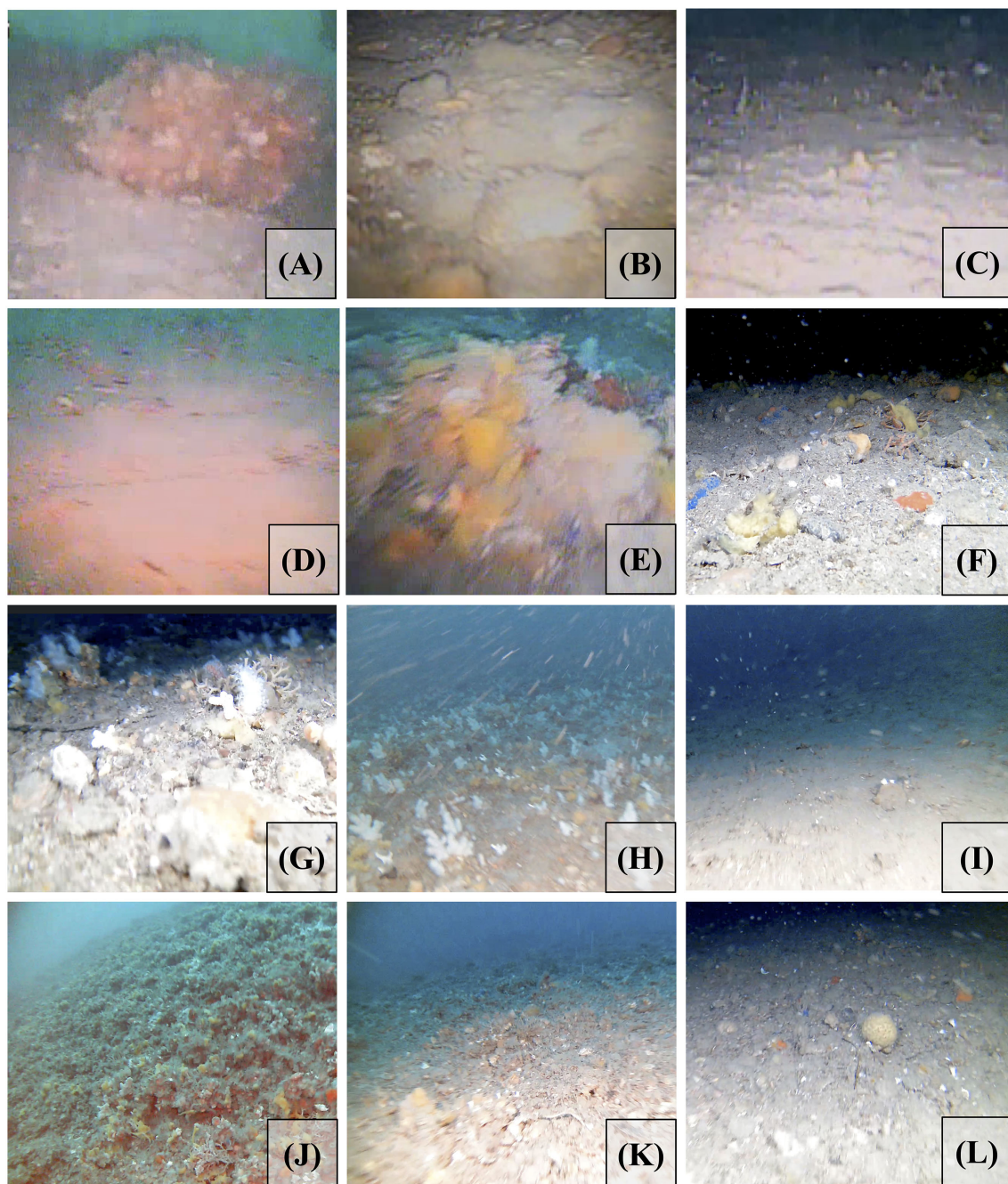
FIGURE 6
Photographs of the sea-bed in the Rion-Antirion Strait area. Panels correspond to different video transects. **(A)** Profile 1. **(B)** Profile 2. **(C)** Profile 3. **(D)** Profile 4. **(E)** Profile 5 and 6. **(F)** Profile 7 and 8. **(G)** Profile 9, image 1 (before the *Alcyonium* spp. field). **(H)** Profile 9, image 2 (inside the *Alcyonium* spp. field). **(I)** Profile 10. **(J)** Profile 11, image 1 (during the mount). **(K)** Profile 11, image 2 (after the mount). **(L)** Profile 12.

and *Axinyssa* spp., although densities were lower than in shallower settings. Thin calcified stems of Antipatharia and perfectly preserved dead bryozoan branches further attest to recent mortality.

In the western moat and plateau megahabitat (profile 5), the 80-m deep moat comprised coarse sand, rubble patches, and scattered boulders colonized by sponges and occasional *Halocynthia papillosa* (Figure 3). Antipatharians and *Alcyonium* spp. appeared on boulders near the moat margin (Figure 4C). On the 60 m deep

plateau, boulders beared sponges, while flatter sandy areas hosted locally dense *Alcyonium* spp. and sponge fields. Uniform colony size of *Alcyonium* spp. and millimetric yellow *Axinyssa* spp. sponges was observed. A 10 cm-high bryozoan colony was documented (Figure 5G). Profile 6 confirms this pattern on the plateau, revealing several rubble mounds colonized by *Axinella* spp. and occasional Caryophylliidae spp. (Figure 6), along with a 140 m-long *Alcyonium* high-density field over coarse sand (Figure 3).

In the southwestern plateau – pool macrohabitat (profile 9), between 60 and 80 m, coarse sand punctuated by boulders (Figure 4H) supported Caryophylliidae spp., yellow-orange and black/blue sponges (Figure 3). Flatter zones are densely covered by *Alcyonium* spp., *Axinella* spp., and *Agelas oroides*, forming a 370 m-long high-density coral-sponge field (Figures 4I, 6I). Colony sizes of *Alcyonium* and *Axinyssa*-like sponges are identical to those in profiles 5 and 6 as well as on the submarine cable (Figure 4G), which was probably displaced during the bridge construction. Another bryozoan mound was documented.

Profile 10 extends from the western plateau moat (~80 m) to the southern terrace (~60 m) (Figure 3). The moat edge exhibited bouldery terrain, while its floor alternates rubble–pebble patches (Figures 5E–J) with fine-grained patches covering the sea-floor (Figure 6). The later patches contradicts previously reported coarse carbonate sea-bed sediments (Piper and Panagos, 1979), implying a recent depositional event. Damaged stems of Antipatharia emerge from pebbly areas, whereas clay sectors host only sparse Pennatuloidea bundles. Biodiversity increases near the moat edge where boulders support dense sponge assemblages and Caryophylliidae corals (Figure 4A). It rises again toward the terrace margin, where *Alcyonium*, *Axinella*-like sponges, and *H. papillosa* become common. At 60–65 m on the northern terrace, rugged seafloor is densely colonized by sponges and tunicates, underscoring the biodiversity gradient between the moat and terrace environments.

In the northern terrace (profile 4), at 54 m (Figure 3), a finer grained sediments seabed hosted only four Pennatuloidea spp.; no sponges, tunicates or bryozoans occurred. The absence of biological rubble or hard substrate matches the paucity of living biota, indicating marginal colonization conditions (Figure 6).

In the Eastern plateau and mount macrohabitat (profile 11), between 52 and 70 m (Figure 3), smooth terrain with rubble and low mounds was densely and uniformly colonized by yellow-orange and black sponges, Caryophylliidae corals, with occasional Antipatharia (Figures 5L, 6). This homogeneity was striking. Dead black-coral branches partly overgrown by sponges were also observed (Figure 6), suggesting that the current community may represent a recolonization phase. Starfish attested to broader faunal diversity.

In the eastern channel macrohabitat (profile 1), along the indurated northern wall (60–80 m) (Figures 1, 3, 6), biodiversity was the highest among all profiles. Caryophylliidae spp., *Parazoanthus axinellae*, Antipatharia, Pennatuloidea, dense *Axinella* patches, and large branching bryozoan colonies thrived in the area. Dead Antipatharia were also present (Figure 4D). At that location, yellow-orange sponges were branched (Figure 5A) and reached heights of more than 15 cm and thickness larger than 1 cm. In sharp contrast, profile 12 on the southeastern channel floor (70–80 m) presented a homogeneous fine grained substrates (probably sandy) bed (Figure 6) with only scattered boulders colonized by *Axinella* and Caryophylliidae spp. This disparity suggests recent dense bottom flows that inhibited recolonization on the channel floor.

In the east basin macrohabitat, very low biotic densities characterized profiles 2 (100 m) and 3 (60 m) (Figure 3). In the depocentre (profile 2), cobbles and boulders were overlain by a recent fine-grained sediment drape (Figure 6)—mirroring the west basin—and hosted only four Pennatuloidea, one *Alcyonium*, and a few possible stems of Antipatharia. The *Alcyonium* specimens at that location had a size similar to the one on the plateau megahabitat, suggesting a similar age. Along the basin margin (profile 3), fine-grained sediments with dead calcareous stems suggests another mortality record (Figure 6); the living fauna was limited to seven Pennatuloidea colonies and one unidentified yellow sponge.

Together, these morphological and biological observations provide the basis for assessing the drivers of recent disturbance and recovery, discussed in Section 5.

3.5 Hydrodynamics and nutrient supply

Our hydrodynamic modeling provides estimates of temperature, current direction, and intensity in the Rion-Antirion Strait. Bottom water temperatures ranges from 14°C to 18°C, with warmer water masses in the northern Strait, where depths are shallower (0–50 m). Average bottom currents (Figure 7) range from 0.01 to 0.25 m/s and are directed southwest towards Patras.

We also computed maximum current speeds for 2019. As shown in Figure 7, these range from 0.1 to 0.8 m/s, with the strongest located just northeast of the bridge. This pattern indicates that the strongest hydrodynamic activity occurs in the center of the Strait, which aligns with the coarsest sediments observed there (Piper and Panagos, 1979), and the finding of the underwater visual inspection of this survey. The maximum current distribution largely mirrors that of average speeds, except in the east basin, where maxima trend northeast. The highest velocities are on the plateau megahabitat and decline more sharply toward the east basin than the west one. Similarly, just west of the bridge, there is a marked northward decrease in bottom velocity, coinciding with a change in seabed grain size suggested by profile comparison (profile 10 vs. profile 4), and a shift in current direction. Maximum velocities exhibit more abrupt spatial variation than average velocities during May 2019 (Rubi et al., 2022). These fluctuations may cause turbulence, vertical mixing, and seafloor erosion.

To investigate tidal-driven variability in current direction, as previously noted in Rubi et al. (2022), we plotted bottom current intensity and direction for May 2019 at the Strait center (31.32°N, 21.78°E) in Figure 8. The diagram shows hourly distributions of horizontal (u) and vertical (v) velocities (745 points). A clear trend emerges: most currents are oriented southwest, exiting the Strait. In contrast, the eastern part exhibits more scattered directions and intensities, implying a prevailing transport toward the west basin megahabitat, which contains observed rubble accumulations.

In addition to the physical parameters described above, we examined indicators of local primary productivity. A higher chlorophyll content (Figure 9) was observed in the Strait compared to the two gulfs. This suggests enhanced nutrient supply and primary productivity within the Strait, likely promoted by strong hydrodynamics and vertical mixing. Such conditions may help sustain benthic suspension feeders, including corals, sponges, and bryozoans, despite frequent disturbances.
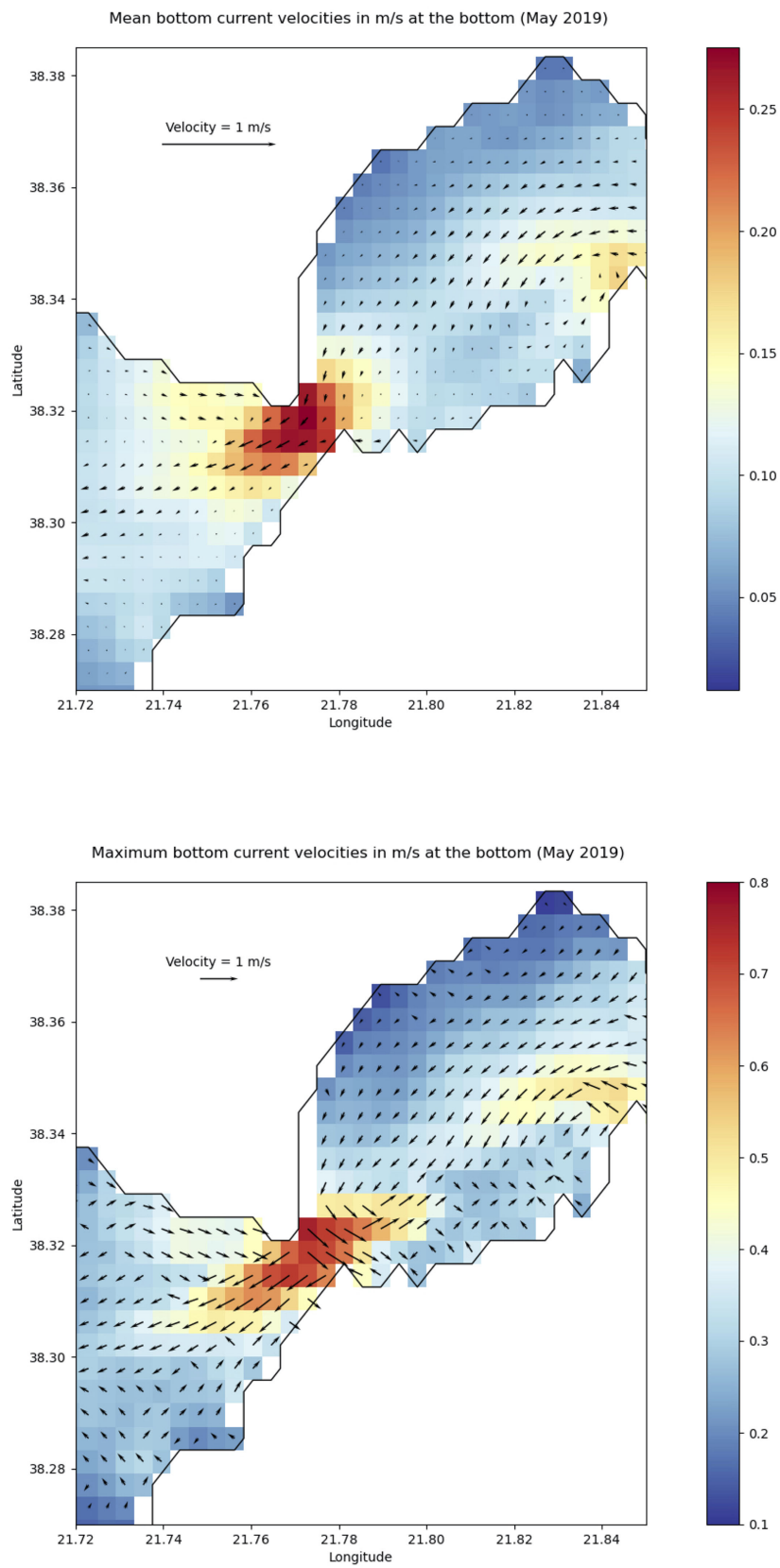
FIGURE 7
Top: mean direction and intensity (m/s) of bottom currents in the Rion-Antirion Strait during May 2019. Bottom: direction and intensity of the strongest bottom currents for the same period.
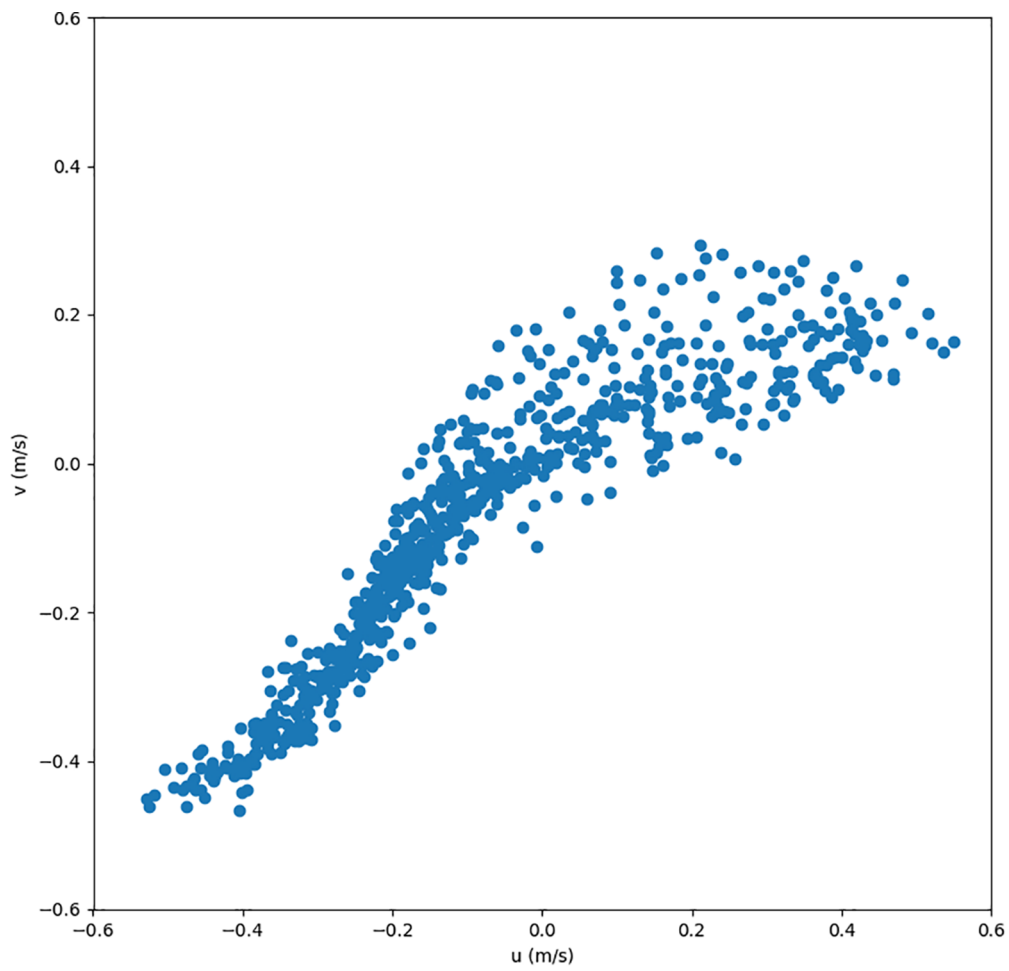
FIGURE 8
Hourly intensity and direction of bottom currents at the center of the strait (31.32°N, 21.78°E) throughout May 2019.
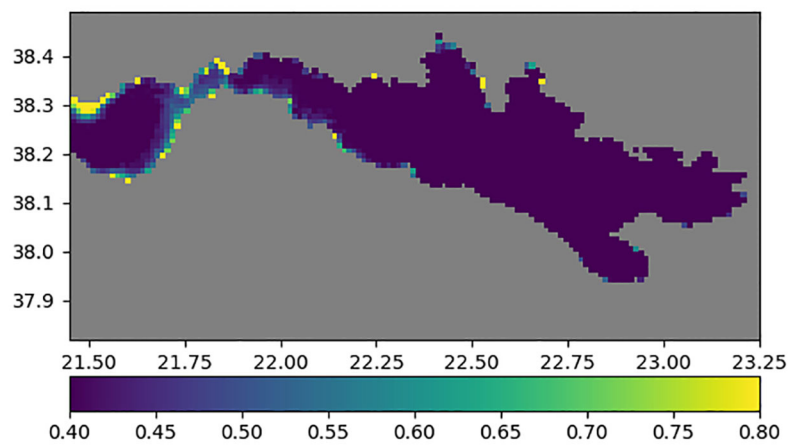

FIGURE 9
Mean chlorophyll-a concentration (mg/m³) from 2008 to 2022, highlighting increased values in the strait area between the Gulfs of Corinth and Patras. Axes show longitude (x) and latitude (y) in decimal degrees.

4 Discussion

4.1 Potential anthropogenic impact on the biotope

Bridge construction (1998–2004) imposed the most intense short-term anthropogenic disturbance ever recorded in the Strait. Extensive engineering works aimed at securing the site against seismic risk included seabed levelling, excavation around piles M1–M4 (Figure 1), and dockyard dredging (Biesiadecki et al., 2004). These activities profoundly modified both the substrate and the water column, generating coarse and fine sediment releases that impacted benthic communities.

We foresee two main processes that could have affected the MAFs and caused the observed large-scale mortality event. First, coarse materials introduced during seabed excavation, levelling, and bridge pier ballasting were likely mobilized by strong bottom currents exceeding 1 m s^{-1} (Figures 7, 8). Once set in motion, these coarse fragments would have been transported across the plateau through rolling and siltation. This process mechanically damaged the benthic assemblages, buried organisms, and disrupted habitats. Some fragments may have eventually accumulated in the basins (profiles 7 and 8; Figure 6). Second, finer sediments were released primarily at the M4 pile—where the upper sedimentary sequence was excavated—and at the M3 pile, where a >10 m-thick clay layer underlies the indurated sandy plateau (3–5 m thick) (Figure 1). Their resuspension and redistribution by the intense hydrodynamics of the Strait likely generated widespread high-turbidity events in the water column that may trigger density currents. These events would have further reduced light penetration, clogged the aquiferous systems of filter feeders, and potentially lowered oxygen levels, creating conditions that were less favorable for benthic organisms in the following years.

Such disturbances are consistent with evidence for a recent, severe mortality event in the Strait. This is exemplified by the widespread occurrence of well-preserved dead biogenic debris — mainly broken bryozoans, anthozoans branches and sponge fragments (profile 8; Figure 5) — showing little erosion and indicating a recent mass mortality (Figure 6F). In addition, coarse rubble composed of numerous pebbles, cobbles, and occasional boulders occurs on the plateau close to the bridge, where it is more frequent than in other megahabitats (profile 9; profile 5; profile 6; profile 11; Figures 6G, E, K). This grain size is different from the sand-rich lithology revealed by boreholes at the bridge site (Biesiadecki et al., 2004), suggesting that these clasts were locally derived during construction and subsequently reworked by strong currents. Together, these observations indicate a combination of mechanical destruction and sediment reworking associated with the bridge works, providing physical evidence for the disturbance that affected the MAFs. Finally, two main observations point to post-disturbance recovery. First, the uniformly small sizes of coral colonies and sponges (Figures 5L, 6H, J) on nearly all habitats and on the cable (profile 9; Figure 4G) suggest a cohort likely established simultaneously, consistent with recruitment after a disturbance. Second, east of the bridge (profile 11), thin calcified

stems of Antipatharia partly overgrown by sponges indicate a former assemblage likely destroyed by a major mortality event, with current communities representing a recolonization phase.

Regarding the biogenic debris observed in the western basin, a key question is whether they represent *in situ* destruction of local assemblages or transported remains from the vicinity of the bridge piers. The preservation of delicate biogenic fragments, together with the presence of a fine-grained sediment drape draping these deposits, indicates limited transport and supports an *in situ* origin for most of the debris. The fine-grained sediment drape likely formed shortly after the mortality event, as suspended sediments released during construction settled under reduced hydrodynamic conditions, preserving the underlying biological material. This interpretation is consistent with the absence of coarse debris trails or erosional features that would suggest downslope displacement.

Other local observations of fine-grained deposits further indicate that construction activities reworked and redistributed sediments across the Strait. Recent fine-grained sediment drapes above rubble also occur in the eastern basin (profiles 2–3), whereas in the western basin they are more localized. Sediment draping occurring where currents weaken (Figures 7, 8) is consistent with post-disturbance resuspension and re-sedimentation under low-energy conditions. The thin veneer deposits of fine-grained sediments above rubbles are more consistent with a single depositional event linked to bridge works rather than a continuous fluvial input from rivers. There are no significant rivers nearby, and the presence of these fine sediments contradicts pre-construction surveys by Piper and Panagos (1979), which reported the absence of fine-grained material in the Strait. By contrast, fine-grained surficial deposits patches in the western moat (profile 5) and fine sands in the eastern channel (profile 12)—both close to the bridge—point to high turbidity currents triggered by excavation. In these areas, biodiversity remains very low, consistent with a strong local impact.

The prolonged suspension of fine sediments would have increased turbidity throughout the Strait. CTD casts from 2000 (Figure 2), recorded during the early stages of bridge construction, show unexpectedly dissolved-oxygen values lower than in the Gulf of Patras and different from supersaturation reported prior to the bridge works (Friligos et al., 1985). This suggests that suspended organic-rich particles may have fueled microbial respiration (Rhoads, 1973), enhancing oxygen consumption. Such conditions are known to stress corals and other suspension feeders (Freiwald et al., 2004), which may have influenced the invertebrate recolonization in the Strait.

4.2 Post-disturbance recolonization patterns

Contrary to expectations of a more pronounced impact immediately adjacent to the bridge piers, the present-day MAF appears more developed on the terrace than in the two adjacent basins, suggesting that recolonization has been more successful on the terrace megahabitat despite its proximity to the construction

site. On the terrace (Figure 1; profile 10), video footage reveals uniformly small, even-aged colonies of *Alcyonium* and millimeter-scale yellow sponges, indicative of a single post-construction recruitment pulse (profile 9; Figure 6H). These early-successional assemblages are dominated by sponge–coral–tunicate associations west of the bridge (profile 9; Figure 6G; Figure 4G) and mostly sponges east of the bridge (Profile 11; Figure 6J). Sponges likely play a structuring role, offering protected microhabitats for coral larvae to settle in the high-energy environment. At greater depths, in the east and west basins, recolonization remains incomplete. Persistent barren patches – such as the eastern half of profile 8 (Figure 3) – suggest that local environmental constraints continue to impede full recovery two decades after the disturbance.

We hypothesize that the terrace may have undergone partial recolonization by similar benthic assemblages originating from nearby "refuge" mesohabitats. The most plausible "refuge" habitat is the northern part of the Eastern Channel, the most sheltered area of the Strait. This zone exhibits fewer biogenic rubble but supports the most diverse benthic community with colonies of varying sizes (profile 1; Figure 3). We infer that this benthic community is the oldest because *Axinella* spp. branching sponges attain heights of ≈ 20 cm and show a more complex branching pattern, suggesting longer growth (Profile 1; Figure 5A), whereas in other areas, colonies are only a few centimeters high and display simpler morphologies (profile 9; Figure 4H). This mesohabitat could have acted as a source of propagules for recolonization after the disturbance.

Substrate modifications introduced during construction also likely condition these trajectories. Coarse debris blocks – probably related to ballast or excavated rock – now host dense sponge–coral associations, whereas deposits of fine construction-derived sediments, notably on the Eastern Channel floor (profile 12) and parts of the western moat (profile 5), support little or no benthic life. Hydrodynamic and sedimentary alterations generated by the bridge appear long-lived. ADCP data collected in 2019 show sustained high turbidity within the strait (Rubi et al., 2022). Fine particles start to settle over lower-energy substrates in the west and east basins (profiles 8 and 2–3), potentially converting former coral habitats into unfavorable soft-bottom facies (Mienis et al., 2007; Davies et al., 2009; Rebesco and Taviani, 2019; Portilho-Ramos et al., 2022).

Most of the invertebrate species recorded in this study have been previously documented from the Gulf of Corinth and nearby waters of the Ionian and Aegean Seas, being common in dim-light environments (e.g., Salomidi et al., 2006; Çinar et al., 2020; Stamouli et al., 2023). Comparison with a less disturbed reference site on the shallower rocky southern slope of the Gulf of Corinth (Salomidi et al., 2006; Çinar et al., 2020) highlights the scale of impact: that site hosts a rich benthic community, including abundant gorgonians, diverse scleractinians, bryozoans, sponges, echinoderms, molluscs and fishes. Even if this site differs substantially in environmental setting, the comparison evidence the lack of almost all motile epifauna and the markedly reduced diversity in the Strait. We therefore infer only partial recovery, the trajectory constrained by (i) mechanical damage from coarse-sediment mobilization, (ii) prolonged turbidity and fine-sediment burial, and (iii) secondary

oxygen depletion. Together, these stressors have likely produced a long-lasting anthropogenic shift in benthic community structure in the Rion–Antirion Strait.

In addition to biological mechanisms, the physical environment of the Strait itself contributes to ecosystem resilience. Elevated chlorophyll concentrations compared to the adjacent gulfs (Figure 9) indicate higher primary productivity, consistent with vigorous local hydrodynamics (Figure 7). Strong bidirectional currents, driven by marine and internal tides, enhance nutrient cycling and sediment resuspension, while the strait's bathymetry promotes the upsloping of cold, nutrient-rich Corinthian waters into the photic zone, a process amplified by internal wave activity. Together, these processes create optimal conditions for phytoplankton growth and ensure a sustained supply of food particles to suspension feeders. Such favorable background conditions likely facilitate coral and sponge recolonization, mitigating long-term disturbance impacts and underpinning the resilience mechanisms discussed in the following section.

4.3 Resilience

The Rion-Antirion Bridge construction provides a unique opportunity to examine species resilience in the Strait. Sponges, tunicates, and dead frameworks play a central role in this process by increasing habitat complexity. This structural heterogeneity provides suitable microhabitats for coral larvae settlement (Whalan et al., 2015; Kazanidis et al., 2021). On a microlocal scale (< 1 cm, Levenstein et al., 2022), sponges offer shelter that allows larvae to settle without being displaced by currents – an essential factor in such a dynamic environment. Additionally, sponges can indirectly promote larval settlement by producing biofilms, which are preferred substrates for anthozoans larvae (Whalan and Webster, 2014).

Dead frameworks (e.g., <10 m structures) also act as habitats for anthozoans development (Rebesco and Taviani, 2019). Composed of coral branches with biofilm, epifauna, and endofauna (De Froe et al., 2019), these frameworks support microbial activity that contributes to nutrient cycling and biofilm development (Maier et al., 2021). Such conditions enhance settlement by offering chemically and structurally favorable substrates (Davies et al., 2009; Davies and Guinotte, 2011; Rebesco and Taviani, 2019; Maier et al., 2020; Portilho-Ramos et al., 2022). Sponges and tunicates, as filter-feeding organisms, further contribute to the remineralization of organic matter and can exhibit trophic complementarity. In deep-sea coral ecosystems, they recycle dissolved organic matter (DOM) expelled by corals via the "sponge loop" (Rix et al., 2016). Together, these groups play a critical role in biogeochemical cycling, increasing the availability of local resources necessary for coral growth and survival, and thereby supporting the resilience of MAF ecosystems in the Rion-Antirion Strait (Henry and Roberts, 2017; Maier et al., 2020; Kazanidis et al., 2021; Reigel et al., 2024).

Anthozoan communities themselves show clear differences in density (Figure 3), which can be interpreted as reflecting species-

specific resilience. Dominant species include *Alcyonium* spp. and Caryophylliidae spp. (Figure 3), considered pioneer taxa due to their ability to rapidly colonize available substrates and adapt to changing conditions. *Alcyonium* spp. forms extensive fields (Figure 4) which can be explained by several factors. Their flexible feeding strategy allows them to assimilate phytoplankton, zooplankton, and DOM (Garrabou, 1999; Budd, 2008), while their dual reproductive strategy – sexual (broadcast spawning) and asexual (fragmentation) – supports rapid expansion (McFadden, 1997; Reynaud and Ferrier-Pagès, 2019). The observed dense monospecific fields may result from fragmentation triggered by construction, with fragments settling on suitable substrates and growing into new colonies under favorable conditions (Reynaud and Ferrier-Pagès, 2019). *Alcyonium* spp. also tolerates turbidity through active contraction of their polyps (Budd, 2008; Rizzo et al., 2021), although high turbidity still slows growth (Larsson and Purser, 2011), explaining their relatively low height.

Caryophylliidae spp. are consistently present across most transects. These characteristic scleractinian corals of the Strait have also been recorded in Holocene marine cores from Nafpaktos Bay (Hubert-Ferrari, personal communication). Their resilience is likely linked to their hard skeletons and small size (~1 cm), which confer robustness against strong currents. They tolerate oligotrophic environments (Roder et al., 2013) and reproduce both sexually and asexually (Marchini et al., 2022), strategies well-suited to local conditions.

By contrast, Pennatuloidea and Antipatharia are sparse (Figure 3) and degraded. These vulnerable taxa show limited recolonization post-construction. Both groups are recognized as VMEs (Vulnerable Marine Ecosystems) (Lastras et al., 2016; Lauria et al., 2017; Buhl-Mortensen et al., 2019; Terzin et al., 2021; Portilho-Ramos et al., 2022), and their poor survival suggests the need for targeted conservation strategies.

5 Conclusions

This study documents, for the first time, a rich and original anthozoan–sponge–tunicate MAF biotope in the Rion–Antirion Strait, developing on gravelly and sandy seabeds (semi-firm substrate), hosting several VME-indicator and protected taxa (e.g., *Axinella* spp., *Tethya citrina*, *Antipathella subpinnata*, Caryophyllidae spp.) (Rizzo et al., 2025).

The formation and persistence of this biotope are fostered by the strait's unique hydrodynamic regime, characterized by strong, reversing bottom currents that enhance food supply and prevent sediment smothering. This assemblage represents the main living biotope of the Strait, while other groups such as bryozoans (mostly represented by dead branches), holothurians, benthic fish, and asterozoans occur only sporadically and do not seem to structure the community.

The results also reveal the lasting impact of large-scale engineering works linked to the Rion–Antirion Bridge, which likely caused extensive habitat alteration through dredging, dumping, and sediment resuspension. Two decades later,

recolonization is dominated by pioneer taxa such as *Alcyonium* spp. and small scleractinians (Caryophylliidae spp.), whose success reflects opportunistic feeding modes and reproductive plasticity. In contrast, the scarcity of fragile or slow-growing species such as pennatulaceans, and black anthozoans underlines the long recovery times these species likely require after acute disturbance.

The absence of pre-disturbance data (pre-1998) limits precise quantification of biodiversity loss; nonetheless, this study sheds light on the ecological processes driving community reassembly in high-energy settings. These findings highlight the ecological value of the Rion–Antirion Strait as a distinctive Mediterranean habitat for MAFs and their associated fauna and emphasize the need for continued monitoring to assess long-term ecosystem trajectories in areas subjected to intense anthropogenic pressure.

Data availability statement

The original contributions presented in the study are included in the article/Supplementary Material. Further inquiries can be directed to the corresponding author.

Author contributions

LT: Investigation, Visualization, Writing – original draft, Data curation, Conceptualization. AH-F: Funding acquisition, Project administration, Conceptualization, Supervision, Writing – review & editing. BC: Methodology, Writing – review & editing, Data curation, Visualization, Formal Analysis, Software. VG: Validation, Writing – review & editing. DC: Resources, Data curation, Writing – review & editing, Investigation. EF: Data curation, Resources, Investigation, Writing – review & editing. XD: Investigation, Writing – review & editing, Data curation, Resources. MG: Resources, Investigation, Writing – review & editing, Data curation. GP: Data curation, Writing – review & editing, Resources, Investigation.

Funding

Acknowledgments

campaign. We acknowledge the contributions of the students who participated in the field mission, particularly Stefania Mylona and Alkiviadis Kontos.

Conflict of interest

The authors declare that the research was conducted in the absence of any commercial or financial relationships that could be construed as a potential conflict of interest.

Generative AI statement

The author(s) declare that no Generative AI was used in the creation of this manuscript.

Any alternative text (alt text) provided alongside figures in this article has been generated by Frontiers with the support of artificial intelligence and reasonable efforts have been made to ensure accuracy, including review by the authors wherever possible. If you identify any issues, please contact us.

Publisher's note

All claims expressed in this article are solely those of the authors and do not necessarily represent those of their affiliated organizations, or those of the publisher, the editors and the reviewers. Any product that may be evaluated in this article, or claim that may be made by its manufacturer, is not guaranteed or endorsed by the publisher.

References

Álvarez-Pérez, G., Busquets, P., De Mol, B., Sandoval, N. G., Canals, M., and Casamor, J. L. (2005). "Deep-water coral occurrences in the Strait of Gibraltar," in *Cold-water corals and ecosystems*. Eds. A. Freiwald and J. M. Roberts (Springer, Berlin, Heidelberg), 207–221. doi: 10.1007/3-540-27673-4_10

Ambroso, S., Gori, A., Dominguez-Carrió, C., Gili, J.-M., Berganzo, E., Teixidó, N., et al. (2013). Spatial distribution patterns of the soft corals *Alcyonium acaule* and *Alcyonium palmatum* in coastal bottoms (Cap de Creus, northwestern Mediterranean Sea). *Mar. Biol.* 160, 3059–3070. doi: 10.1007/s00227-013-2295-

Anderson, J. J., and Carmack, E. C. (1973). Some physical and chemical properties of the Gulf of Corinth. *Estuar. Coast. Mar. Sci.* 1, 195–202. doi: 10.1016/0302-3524(73)90034-0

André, F., Lamare, V., Reguieg, A., and Sittler, A.-P. (2023). *Halocynthia papillosa (Linnaeus 1767)* (DORIS).

Apostolopoulos, Ch (2010). Coastal bridges and the 120 Life Span – the Rio-Antirio case study. *Int. J. Struct. Integrity* 1, 173–183. doi: 10.1108/17579861011053907

Balogh, V., Fragkopoulou, E., Serrão, E. A., and Assis, J. (2023). A dataset of cold-water coral distribution records. *Data Brief* 48, 109223. doi: 10.1016/j.dib.2023.109223

Barth, A. (2024). NCDatasets.jl: a Julia package for manipulating netCDFdata sets. *JOSS* 9, 6504. doi: 10.21105/joss.06504

Barth, A. (2025). *ROMS.Jl*. Available online at: https://alexander-barth.github.io/ROMS.jl/dev/ (Accessed March 18, 2025).

Beckers, A., Beck, C., Hubert-Ferrari, A., Tripsanas, E., Crouzet, C., Sakellariou, D., et al. (2016). Influence of bottom currents on the sedimentary processes at the western tip of the Gulf of Corinth, Greece. *Mar. Geology* 378, 312–332. doi: 10.1016/j.margeo.2016.03.001

Beckers, A., Hubert-Ferrari, A., Beck, C., Bodeux, S., Tripsanas, E., Sakellariou, D., et al. (2015). Active faulting at the western tip of the Gulf of Corinth, Greece, from high-resolution seismic data. *Mar. Geology* 360, 55–69. doi: 10.1016/j.margeo.2014.12.003

Berning, B. (2007). The Mediterranean bryozoan *Myriapora truncata* (Pallas 1766): a potential indicator of (palaeo-) environmental conditions. *LET* 40, 221–232. doi: 10.1111/j.1502-3931.2007.00019.x

Biesiadecki, G., Dobry, R., Leventis, G., and Peck, R. (2004). "Rion – antirion bridge foundations: A blend of design and construction innovation," in *International Conference on Case Histories in Geotechnical Engineering* (Rolla: University of Missouri-Rolla). Available online at: https://scholarsmine.mst.edu/icchge/5icchge/session00g/14 (Accessed September 15, 2024).

Bramanti, L., Manea, E., Giordano, B., Estaque, T., Bianchimani, O., Richaume, J., et al. (2023). The deep vault: a temporary refuge for temperate gorgonian forests facing marine heat waves. *Mediterr. Mar. Sci.* 24, 601–609. doi: 10.12681/mms.35564

Budd, G. C. (2008). *Dead man's fingers (Alcyonium digitatum): Marine Evidence–based Sensitivity Assessment (MarESA) Review*. (Plymouth: MarLIN – Marine Life Information Network). doi: 10.17031/MARLINSP.1187.1

Buhl-Mortensen, L., Burgos, J. M., Steingrund, P., Buhl-Mortensen, P., Ólafsdóttir, S. H., and Ragnarsson, S.Á. (2019). *Vulnerable marine ecosystems (VMEs)* (Copenhagen: Nordic Council of Ministers), 519. doi: 10.6027/TN2019-519

Caterina, B., Hubert-Ferrari, A., Barth, A., and Beckers, J.-M. (2025). Modelling of the present oceanographic situation of the gulfs of Patras and Corinth. *JMSE* 13, 1827. doi: 10.3390/jmse13091827

Caterina, B., and Hubert-Ferrari, A. (2025). Using 14 years of satellite data to describe the hydrodynamic circulation of the Patras and Corinth gulfs. *J. Mar. Sci. Eng.* doi: 10.3390/jmse13030623

Çinar, M. E., Feral, J. P., Arvanitidis, C., David, R., Taskin, E., Sini, M., et al. (2020). Coralligenous assemblages along their geographical distribution: testing of concepts and implications for management. *Aquat. Conservation: Mar. Freshw. Ecosyst.* 30, 1578–1594. doi: 10.1002/aqc.3365

Combault, J., Morand, P., and Pecker, A. (2000). "Structural response of The Rion-Antirion Bridge," in *Proceedings of the 12th World Conference on Earthquake Engineering* (Upper Hutt: New Zealand Society for Earthquake Engineering). 1609. Available online at: https://www.gefyra.gr/images/user/Publications/Auckland.pdf (Accessed September 15, 2024).

Copernicus Marine Service (2025a). *Mediterranean sea, bio-geo-chemical, L3, daily satellite observations, (1997-ongoing)*. OC-CNR-ROMA-IT. doi: 10.48670/moi-00299

Copernicus Marine Service (2025b). *Mediterranean sea physics reanalysis*. CMCC. doi: 10.25423/CMCC/MEDSEA_MULTIYEAR_PHY_006_004_E3R1

Davies, A. J., Duineveld, G. C. A., Lavaleye, M. S. S., Bergman, M. J. N., van Haren, H., and Roberts, J. M. (2009). Downwelling and deep-water bottom currents as food supply mechanisms to the cold-water coral *Lophelia pertusa* (Scleractinia) at the Mingulay Reef Complex. *Limnol. Oceanogr.* 54, 620–629. doi: 10.4319/lo.2009.54.2.0620

Davies, A. J., and Guinotte, J. M. (2011). Global habitat suitability for framework-forming cold-water corals. *PloS One* 6, e18483. doi: 10.1371/journal.pone.0018483

De Froe, E., Rovelli, L., Glud, R. N., Maier, S. R., Duineveld, G., Mienis, F., et al. (2019). Benthic oxygen and nitrogen exchange on a cold-water coral reef in the north-east atlantic ocean. *Front. Mar. Sci.* 6. doi: 10.3389/fmars.2019.00665

Digenis, M., Akyol, O., Benoit, L., Biel-Cabanelas, M., Çamlik, Ö.Y., Charalampous, K., et al. (2024). New records of rarely reported species in the Mediterranean Sea (March 2024). *Mediterr. Mar. Sci.* 25, 84–115. doi: 10.12681/mms.37214

ECMWF (2018). "MARS - the ECMWF meteorological archive," in *Software and computing services* (ECMWF). Available online at: https://www.ecmwf.int/node/18124.

Egbert, G. D., and Erofeeva, S. Y. (2002). Efficient inverse modeling of barotropic ocean tides. *J. Atmos. Oceanic Technol.* 19, 183–204. doi: 10.1175/1520-0426(2002)019<0183:EIMOBO>2.0.CO;2

Fabri, M. C., Dreidemy, J., Estournel, C., and Vaz, S. (2025). Mapping and Conservation of Cold-Water Corals in the Lacaze-Duthiers Canyon for Transboundary Management . *Mediterranean Marine Science* 26, 349–369. doi: 10.12681/mms.40914

Ferentinos, G., Brooks, M., and Doutsos, T. (1985). Quaternary tectonics in the Gulf of Patras, western Greece. *J. Struct. Geology* 7, 713–717. doi: 10.1016/0191-8141(85)90146-4

Fournier, S., Menot, L., Scavinner, M., and Le Roy, É. (2023). *Guide d'identification des taxons indicateurs d'écosystèmes marins vulnérables* (Atlantique et Méditerranée: EMV). Available online at: https://archimer.ifremer.fr/doc/00834/94627/ (Accessed June 20, 2023).

Fourniotis, N., and Horsch, G. M. (2010). Three-dimensional numerical simulation of wind-induced barotropic circulation in the Gulf of Patras. *Ocean Eng.* 37, 355–364. doi: 10.1016/j.oceaneng.2010.01.002

Fourniotis, N., and Horsch, G. M. (2015). Baroclinic circulation in the gulf of patras (Greece). *Ocean Eng.* 104, 238–248. doi: 10.1016/j.oceaneng.2015.04.080

Fourniotis, N., Horsch, G., and Leftheriotis, G. (2018). On the hydrodynamic geometry of flow-through versus restricted lagoons. *Water* 10, 237. doi: 10.3390/w10030237

Freiwald, A., Fosså, J., Grehan, A., Koslow, T., and Roberts, J. (2004). *Cold-water coral reefs: out of sight – no longer out of mind* (Cambridge, UK: UNEP-WCMC).

Friligos, N., Theocharis, A., and Georgopoulos, D. (1985). Preliminary chemical and physical observations during summer 1980 on a silled embayment in the Ionian Sea. *Vie Milieu/Life Environ.*, 115–125.

Garrabou, J. (1999). Life-history traits of *Alcyonium acaule* and *Parazoanthus axinellae* (Cnidaria, Anthozoa), with emphasis on growth. *Mar. Ecol. Prog. Ser.* 178, 193–204. doi: 10.3354/meps178193

Garrabou, J., Gómez-Gras, D., Medrano, A., Cerrano, C., Ponti, M., Schlegel, R., et al. (2022). Marine heatwaves drive recurrent mass mortalities in the Mediterranean Sea. *Global Change Biol.* 28, 5708–5725. doi: 10.1111/gcb.16301

Garrabou, J., and Harmelin, J. G. (2002). A 20-year study on life-history traits of a harvested long-lived temperate coral in the NW Mediterranean: insights into conservation and management needs. *J. Anim. Ecol.* 71, 966–978. doi: 10.1046/j.1365-2656.2002.00661.x

GEBCO Compilation Group (2023). *GEBCO 2023 grid*. NERC EDS British Oceanographic Data Centre, NOC. doi: 10.5285/f98b053b-0cbc-6c23-e053-6c86abc0af7b

GEBCO Compilation Group (2024). *GEBCO Gridded Bathymetry Data*. https://download.gebco.net/.

Grinyó, J., Garriga, A., Soler-Membrives, A., Santín, A., Ambroso, S., López-González, P. J., et al. (2020). Soft corals assemblages in deep environments of the Menorca Channel (Western Mediterranean Sea). *Prog. Oceanography* 188, 102435. doi: 10.1016/j.pocean.2020.102435

Henry, L.-A., and Roberts, J. M. (2017). "Global biodiversity in cold-water coral reef ecosystems," in *Marine animal forests*. Eds. S. Rossi, L. Bramanti, A. Gori and C. Orejas (Springer International Publishing, Cham), 235–256. doi: 10.1007/978-3-319-21012-4_6

Hinz, H. (2017). "Impact of bottom fishing on animal forests: science, conservation, and fisheries management," in *Marine animal forests*. Eds. S. Rossi, L. Bramanti, A. Gori and C. Orejas (Springer International Publishing, Cham), 1041–1059. doi: 10.1007/978-3-319-21012-4_37

Johnson, M., and Ferreira, J. (2025). Traits and metabolic constraints affect marine animal forest structure. *Mediterr. Mar. Sci.* 26, 370–377. doi: 10.12681/mms.39396

Kazanidis, G., Henry, L.-A., and Roberts, J. M. (2021). Hidden structural heterogeneity enhances marine hotspots' biodiversity. *Coral Reefs* 40, 1615–1630. doi: 10.1007/s00338-021-02114-w

Kefalas, E., and Castritsi-Catharios, J. (2007). Taxonomy of some sponges (Porifera: Demospongiae) collected from the Aegean Sea and description of a new species. *J. Mar. Biol. Ass.* 87, 1527–1538. doi: 10.1017/S002531540705206X

Koletsis, I., Kotroni, V., and Lagouvardos, K. (2013). *A model-based study of the wind regime over Corinthian Gulf in Greece* (NHESS). doi: 10.5194/nhessd-1-2079-2013

Larsson, A. I., and Purser, A. (2011). Sedimentation on the cold-water coral *Lophelia pertusa*: Cleaning efficiency from natural sediments and drill cuttings. *Mar. pollut. Bull.* 62, 1159–1168. doi: 10.1016/j.marpolbul.2011.03.041

Lartaud, F., Mouchi, V., Chapron, L., Meistertzheim, A.-L., and Le Bris, N. (2019). "36 growth patterns of mediterranean calcifying cold-water corals," in *Mediterranean cold-water corals: past, present and future: understanding the deep-sea realms of coral*. Eds. C. Orejas and C. Jiménez (Springer International Publishing, Cham), 405–422. doi: 10.1007/978-3-319-91608-8_36

Lastras, G., Canals, M., Ballesteros, E., Gili, J.-M., and Sanchez-Vidal, A. (2016). Cold-water corals and anthropogenic impacts in la fonera submarine canyon head, northwestern mediterranean sea. *PloS One* 11, e0155729. doi: 10.1371/journal.pone.0155729

Lauria, V., Garofalo, G., Fiorentino, F., Massi, D., Milisenda, G., Piraino, S., et al. (2017). Species distribution models of two critically endangered deep-sea octocorals reveal fishing impacts on vulnerable marine ecosystems in central Mediterranean Sea. *Sci. Rep.* 7, 8049. doi: 10.1038/s41598-017-08386-z

Levenstein, M. A., Gysbers, D. J., Marhaver, K. L., Kattom, S., Tichy, L., Quinlan, Z., et al. (2022). Millimeter-scale topography facilitates coral larval settlement in wave-driven oscillatory flow. *PloS One* 17, e0274088. doi: 10.1371/journal.pone.0274088

Lo Iacono, C., Savini, A., Huvenne, V. A. I., and Gràcia, E. (2019). "15 habitat mapping of cold-water corals in the mediterranean sea," in *Mediterranean cold-water corals: past, present and future: understanding the deep-sea realms of coral*. Eds. C. Orejas and C. Jiménez (Springer International Publishing, Cham), 157–171. doi: 10.1007/978-3-319-91608-8_15

Maier, S. R., Kutti, T., Bannister, R. J., Fang, J. K.-H., Van Breugel, P., Van Rijswijk, P., et al. (2020). Recycling pathways in cold-water coral reefs: Use of dissolved organic matter and bacteria by key suspension feeding taxa. *Sci. Rep.* 10, 9942. doi: 10.1038/s41598-020-66463-2

Maier, S. R., Mienis, F., De Froe, E., Soetaert, K., Lavaleye, M., Duineveld, G., et al. (2021). Reef communities associated with dead' cold-water coral framework drive

resource retention and recycling in the deep sea. *Deep Sea Res. Part I: Oceanographic Res. Papers* 175, 103574. doi: 10.1016/j.dsr.2021.103574

Marchini, C., Fossati, V., Cerpelloni, M., Caroselli, E., Falini, G., Dubinsky, Z., et al. (2022). Sexual reproduction and biometry of the non-zooxanthellate papillose cup coral *Paracyathus pulchellus*. *Front. Mar. Sci.* 9. doi: 10.3389/fmars.2022.925586

McFadden, C. S. (1997). Contribution of sexual and asexual reproduction to population structure in the clonal soft coral, *Alcyonium rudyi*. *Evolution* 51, 112–126. doi: 10.1111/j.1558-5646.1997.tb02393.x

Mienis, F., de Stigter, H. C., White, M., Duineveld, G., de Haas, H., and van Weering, T. C. E. (2007). Hydrodynamic controls on cold-water coral growth and carbonate-mound development at the SW and SE Rockall Trough Margin, NE Atlantic Ocean. *Deep Sea Res. Part I: Oceanographic Res. Papers* 54, 1655–1674. doi: 10.1016/j.dsr.2007.05.013

Mohn, C., Hansen, J. L. S., Carreiro-Silva, M., Cunningham, S. A., De Froe, E., Dominguez-Carrió, C., et al. (2023). Tidal to decadal scale hydrodynamics at two contrasting cold-water coral sites in the Northeast Atlantic. *Prog. Oceanography* 214, 103031. doi: 10.1016/j.pocean.2023.103031

Moore, A. M., Arango, H. G., Broquet, G., Powell, B. S., Weaver, A. T., and Zavala-Garay, J. (2011). The Regional Ocean Modeling System (ROMS) 4-dimensional variational data assimilation systems. *Prog. Oceanography* 91, 34–49. doi: 10.1016/j.pocean.2011.05.004

Mytilineou, Ch., Smith, C. J., Anastasopoulou, A., Papadopoulou, K. N., Christidis, G., Bekas, P., et al. (2014). New cold-water coral occurrences in the Eastern Ionian Sea: Results from experimental long line fishing. *Deep Sea Res. Part II: Topical Stud. Oceanography* 99, 146–157. doi: 10.1016/j.dsr2.2013.07.007

Navionics® (2024). *WebApp navionics chartViewer*. Available online at: https://maps.garmin.com/fr-BE/marine/ (Accessed September 20, 2024).

Orejas, C., Carreiro-Silva, M., Mohn, C., Reimer, J. D., Samaai, T., Allcock, A., et al. (2022). Marine animal forests of the world: definition and characteristics. *Res. Ideas Outcomes* 8, e96274. doi: 10.3897/rio.8.e96274

M. Otero and C. Mytilineou (Eds.) (2022). "Deep-sea Atlas of the eastern Mediterranean Sea," in *IUCN-HCMR deepEastMed project* (IUCN, Gland, Malaga), VII–371.

Piper, D. J. W., and Panagos, A. G. (1979). *Surficial sediments of the Gulf of Patras*. Available online at: http://hdl.handle.net/123456789/222https://okeanos-dspace.hcmr.gr/xmlui/handle/123456789/222.

Portilho-Ramos, R., da, C., Titschack, J., Wienberg, C., Rojas, M. G. S., Yokoyama, Y., et al. (2022). Major environmental drivers determining life and death of cold-water corals through time. *PloS Biol.* 20, e3001628. doi: 10.1371/journal.pbio.3001628

Poulos, S. E., Collins, M. B., Pattiaratchi, C., Cramp, A., Gull, W., Tsimplis, M., et al. (1996). Oceanography and sedimentation in the semi-enclosed, deep-water Gulf of Corinth (Greece). *Mar. Geology* 134, 213–235. doi: 10.1016/0025-3227(96)00028-X

Rebesco, M., and Taviani, M. (2019). "4 A turbulent story: mediterranean contourites and cold-water corals," in *Mediterranean cold-water corals: past, present and future: understanding the deep-sea realms of coral*. Eds. C. Orejas and C. Jiménez (Springer International Publishing, Cham), 35–46. doi: 10.1007/978-3-319-91608-8_4

Reigel, A. M., Easson, C. G., Apprill, A., Freeman, C. J., Bartley, M. M., and Fiore, C. L. (2024). Sponge-derived matter is assimilated by coral holobionts. *Commun. Biol.* 7, 146. doi: 10.1038/s42003-024-05836-z

Reynaud, S., and Ferrier-Pagès, C. (2019). "Biology and ecophysiology of mediterranean cold–water corals," in *Mediterranean cold-water corals: past, present and future*. Eds. C. Orejas and C. Jiménez (Springer International Publishing, Cham), 391–404. doi: 10.1007/978-3-319-91608-8_35

Rhoads, D. C. (1973). The influence of deposit-feeding benthos on water turbidity and nutrient recycling. *Am. J. Sci.* 273, 1–22. doi: 10.2475/ajs.273.1.1

Rix, L., De Goeij, J. M., Mueller, C. E., Struck, U., Middelburg, J. J., Van Duyl, F. C., et al. (2016). Coral mucus fuels the sponge loop in warm- and cold-water coral reef ecosystems. *Sci. Rep.* 6, 18715. doi: 10.1038/srep18715

Rizzo, L., Fiorillo, I., and Rossi, S. (2021). Seasonal trends of the polyp expansion and nutritional condition of *Alcyonium acaule* (Octocorallia, Alcyonacea). *PeerJ* 9, e12032. doi: 10.7717/peerj.12032

Rizzo, L., Vega Fernández, T., Necci, F., Grelaud, M., Ziveri, P., Gerovasileiou, V., et al. (2025). Can Marine Animal Forests benefit from existing conservation measures? A systematic approach towards the identification of protected sessile benthic species in the Mediterranean Sea. *Mediterr. Mar. Sci.* 26, 327–340. doi: 10.12681/mms.38550

Roder, C., Berumen, M. L., Bouwmeester, J., Papathanassiou, E., Al-Suwailem, A., and Voolstra, C. R. (2013). First biological measurements of deep-sea corals from the Red Sea. *Sci. Rep.* 3, 2802. doi: 10.1038/srep02802

Rossi, S., Bramanti, L., Costantini, F., Dailianis, T., Schubert, N., and Gerovasileiou, V. (2025). Marine animal forests: bridging science, policy, and local knowledge. *Mediterr. Mar. Sci.* 26, 418–420. doi: 10.12681/mms.40440

Rossi, S., Bramanti, L., Gori, A., and Orejas, C. (2017). "An overview of the animal forests of the world," in *Marine animal forests*. Eds. S. Rossi, L. Bramanti, A. Gori and C. Orejas (Springer International Publishing, Cham), 1–26.

Rowley, S. J. (2008). "*Ascidia mentula* A sea squirt," in *Marine life information network: biology and sensitivity key information reviews, [on-line]*. Eds. H. Tyler-Walters and K. Hiscock (Marine Biological Association of the United Kingdom, Plymouth). Available online at: https://www.marlin.ac.uk/species/detail/8 (Accessed December 05, 2024).

Rubi, R., Hubert-Ferrari, A., Fakiris, E., Christodoulou, D., Dimas, X., Geraga, M., et al. (2022). Hydrodynamics and sedimentary processes in the modern Rion strait (Greece): Interplay between tidal currents and internal tides. *Mar. Geology* 446, 106771. doi: 10.1016/j.margeo.2022.106771

Rueda, J. L., Urra, J., Aguilar, R., Angeletti, L., Bo, M., García-Ruiz, C., et al. (2019). "29 cold-water coral associated fauna in the mediterranean sea and adjacent areas," in *Mediterranean cold-water corals: past, present and future: understanding the deep-sea realms of coral*. Eds. C. Orejas and C. Jiménez (Springer International Publishing, Cham), 295–333. doi: 10.1007/978-3-319-91608-8_29

Salomidi, M., Issaris, Y., and Pancucci-Papadopoulou, M. A. (2006). "Marine protected areas as a coastal management tool: feasibility study in a biodiversity hotspot," in *Proceedings of the 8th Panhellenic Symposium on Oceanography and Fisheries* (Athens: HCMR Publ.). Thessaloniki, 4–6 June 2006. 663–668.

Salomidi, M., Marchiò, A., Issaris, Y., Gerakaris, V., Dailianis, T., and Gerovasileiou, V. (2025). Advancing knowledge on red coral *Corallium rubrum* (Linnaeus 1758) populations and associated mesophotic communities in the Aegean Sea, Eastern Mediterranean. *Mediterr. Mar. Sci.* 26, 378–392. doi: 10.12681/mms.41403

Salomidi, M., Smith, C., Katsanevakis, S., Panayotidis, P., and Papathanasiou, V. (2009). "Some observations on the structure and distribution of gorgonian assemblages in the eastern Mediterranean Sea," in *Proceedings of the 1st Symposium on the Conservation of Coralligenous and Other Bio-Concretions in the Mediterranean Sea* (Tunis: RAC/SPA Publ.). 242–245.

SeaDataNet (2000). *INTERREG II - interreg ionian (INTERREG II)* (SeaDataNet/ EDMERP). Available online at: https://edmed.seadatanet.org/report/1301/ (Accessed September 17, 2024).

Shchepetkin, A. F., and McWilliams, J. C. (2005). The regional oceanic modeling system (ROMS): a split-explicit, free-surface, topography-following-coordinate oceanic model. *Ocean Model.* 9, 347–404. doi: 10.1016/j.ocemod.2004.08.002

Shchepetkin, A. F., and McWilliams, J. C. (2009). Correction and commentary for "Ocean forecasting in terrain-following coordinates: Formulation and skill assessment of the regional ocean modeling system" by Haidvogel et al. J. Comp. Phys. 227, pp. 3595–3624. *J. Comput. Phys.* 228, 8985–9000. doi: 10.1016/j.jcp.2009.09.002

Stamouli, C., Gerovasileiou, V., and Voultsiadou, E. (2023). Sponge community patterns in mesophotic and deep-sea habitats in the aegean and ionian seas. *JMSE* 11, 2204. doi: 10.3390/jmse11112204

Stow, D. A. V., Hernández-Molina, F. J., Llave, E., Sayago-Gil, M., Díaz Del Río, V., and Branson, A. (2009). Bedform-velocity matrix: The estimation of bottom current velocity from bedform observations. *Geology* 37, 327–330. doi: 10.1130/G25259A.1

Taviani, M., Angeletti, L., Antolini, B., Ceregato, A., Froglia, C., López Correa, M., et al. (2011). Geo-biology of Mediterranean deep-water coral ecosystems. *Mar. Res. at CNR* 6, 705–719.

Taviani, M., Angeletti, L., Canese, S., Cannas, R., Cardone, F., Cau, A., et al. (2017). "The " Sardinian cold-water coral province " in the context of the Mediterranean coral ecosystems," in *Deep sea research part II topical studies in oceanography*.

Terzin, M., Paletta, M. G., Matterson, K., Coppari, M., Bavestrello, G., Abbiati, M., et al. (2021). Population genomic structure of the black coral *Antipathella subpinnata* in Mediterranean Vulnerable Marine Ecosystems. *Coral Reefs* 40, 751–766. doi: 10.1007/s00338-021-02078-x

Thurstan, R. H., Pandolfi, J. M., and Zu Ermgassen, P. S. E. (2017). "Animal forests through time: historical data to understand present changes in marine ecosystems," in *Marine animal forests*. Eds. S. Rossi, L. Bramanti, A. Gori and C. Orejas (Springer International Publishing, Cham), 947–963. doi: 10.1007/978-3-319-21012-4_31

UNEP/MAP–SPA/RAC (2023). *Greece: Conservation of Mediterranean marine and coastal biodiversity by 2030 and beyond* (Tunis: Specially Protected Areas Regional Activity Centre (SPA/RAC).

Whalan, S., Abdul Wahab, M. A., Sprungala, S., Poole, A. J., and De Nys, R. (2015). Larval settlement: the role of surface topography for sessile coral reef invertebrates. *PloS One* 10, e0117675. doi: 10.1371/journal.pone.0117675

Whalan, S., and Webster, N. S. (2014). Sponge larval settlement cues: the role of microbial biofilms in a warming ocean. *Sci. Rep.* 4, 4072. doi: 10.1038/srep04072

WikiROMS (2019). *Vertical S-coordinate* (WikiROMS). Available online at: https://www.myroms.org/wiki/Vertical_S-coordinate (Accessed September 09, 2025).

WoRMS Editorial Board (2025). *World register of marine species* (VLIZ). Available online at: http://www.marinespecies.org.